THE UNIVERSITY OF SYDNEY

FORMULATION AND IMPLEMENTATION OF GENERAL THIN-WALLED OPEN-SECTION BEAM-COLUMN ELEMENTS IN OPENSEES

RESEARCH REPORT R961

RINCHEN

GREGORY J. HANCOCK

KIM J.R. RASMUSSEN

February 2016

Copyright Notice

Acknowledgement

ABSTRACT

The formulation and implementation of beam-column finite elements for the general thin-walled open cross-sections within the OpenSees framework is presented. To account for the non-coincident location of shear centre and centroid as is the case in non-symmetric sections, a local cross-section transformation matrix is derived relating the axial force acting through the centroid and the shear centre. The stiffness relations are derived based on the Green-Lagrange strain for the displacement-based beam-column element while the Wagner effect is incorporated in the torsional rigidity term for the elastic beam-column element. The beam-column elements are then implemented within the co-rotational framework of OpenSees. The performance of developed beam-column elements are demonstrated through the use of monosymmetric, doubly-symmetric and asymmetric sections in a series of numerical examples. The solutions obtained are verified with the results from the beam and shell element models in ABAQUS software.

KEYWORDS

Centroid, shear centre, warping, monosymmetric, asymmetric, thin-walled open sections, post-buckling, co-rotation, nonlinear analysis

TABLE OF CONTENTS

1. INTRODUCTION

Thin-walled cold-formed steel sections are widely used in light gauge constructions such as industrial warehouses, sheds, and in relatively short span portal frames. However, the structural behaviour of thin-walled open sections is rather complex mainly owing to their low torsional rigidity and propensity to buckle and warp. Quite often the shear centre and the centroid are non-coincident as in monosymmetric or asymmetric sections. In some sections, such as in channel sections, the shear centre and the centroid are both located outside the material point. Six degrees of freedom commonly used in the solid sections is often not adequate to completely define the deformation of thin-walled open sections as they are prone to warping. All these factors must be taken into account when formulating the finite element of beams with open cross-sections.

Over the years, several researchers have made significant contribution towards the theoretical and numerical modelling of thin-walled sections. Baigent and Hancock [1] and Hancock [2] formulated the matrix displacement method incorporating the warping torsion for the linear elastic analysis of general thin-walled sections. They also introduced warping as the 7th degree of freedom at the beam ends and successfully implemented for the analysis of single channel-section portal frames. Rasmussen [3] derived the variational equations for general bifurcation analysis of thin-walled members of arbitrary cross-section. Pi and Trahair [4] developed a beam finite element for the prediction of lateral buckling of monosymmetric beam-columns which included the effect of pre-buckling deformation. In the context of large displacement analysis, Gruttmann et al. [5], Hsiao and Lin [6] and Battini and Pacoste [7] formulated the co-rotational beam elements for thin-walled sections with eccentric shear centre and centroid. Alemdar [8] derived the expression for the displacement-based beam-column element in the co-rotational formulation for the doubly symmetric sections. Zhang et al. [9] incorporated the warping degree of freedom in OpenSees [10] and used the method for the nonlinear analysis of doubly symmetric sections.

In this report, the stiffness relations are formulated for the thin-walled beam-column elements with general open cross-sections within the co-rotational framework of OpenSees. To account for the warping of cross-section, the warping degree of freedom is also included in the formulation. Two elements namely an elastic beam-column element(EB) and a displacement based beam-column element(DB) are considered. While the EB element is developed only to validate the solution, the focus has been mainly on the DB element. In terms of displacement functions, both the elastic beam-column elements and the displacement-based beam-column elements use cubic polynomials as interpolation function for transverse displacement and twist, and a linear function for axial displacement. However, the difference lies in the fact that the EB elements are formulated with treatment of each force in isolation and strain terms used are mostly linear while the DB elements take account of the nonlinear Green-Lagrange strain in the formulation. DB elements also have the capability to account for distributed plasticity within the section and along the beam length. However, in this report, the material is assumed to remain linearly elastic throughout the analysis. The formulations are based on Vlasov's kinematics[11] in which the cross-section is assumed to retain its original shape while undergoing overall deformation. The shear deformations due to warping torsion are assumed to be negligible.

As the proposed thin-walled beam-column elements have non-coincident shear centre and centroid, the transformation matrix is developed to take account of the eccentricity of the shear centre and the centroid. The beam-column elements are incorporated in OpenSees and their performance tested through the study of doubly symmetric section, singly symmetric section and asymmetric section subjected to axial compression, bending and torsional loading.

In the sections to follow, brief description of the co-rotational framework is provided followed by outlining the coordinate systems adopted in the formulation. The EB and the DB elements are described next. This is followed by the description of the transformation matrix accounting for the

eccentricity of shear centre and centroid and the transformation from local to global axis systems. Finally, the various benchmark problems using doubly-symmetric, monosymmetric and asymmetric sections are provided to test the performance of the EB and the DB elements developed herein.

2. FORMULATION OF GENERAL THIN-WALLED OPEN SECTION BEAM-COLUMN ELEMENT IN OPENSEES

The co-rotational approach of formulating the nonlinear finite element involves the decomposition of motion of the element into rigid body and pure deformational parts through the use of a reference system which continuously rotates and translates with the element [7,12,13]. The rigid body motions of the element are excluded and only the deformational responses are considered in the stiffness formulation at the local level. However, the geometric nonlinearity induced by the large rigid body motion is captured in the global coordinate system through the transformation matrices relating local and global response quantities.

One of the main features of the co-rotational formulation is its independence on derivation of internal forces and tangent stiffness relations at the local system. The mapping from local to global system remains the same for all types of local elements so long as the element has same number of nodes and degrees of freedom[7].

2.1 Coordinate Systems

2.1.1   Global coordinate systems

In the global coordinate systems, the beam element has 7 degrees of freedom (DoFs) at each end: 3 translations, 3 rotations and 1 warping DoF (Figure 1). The sign of the rotations follows the right hand rule.
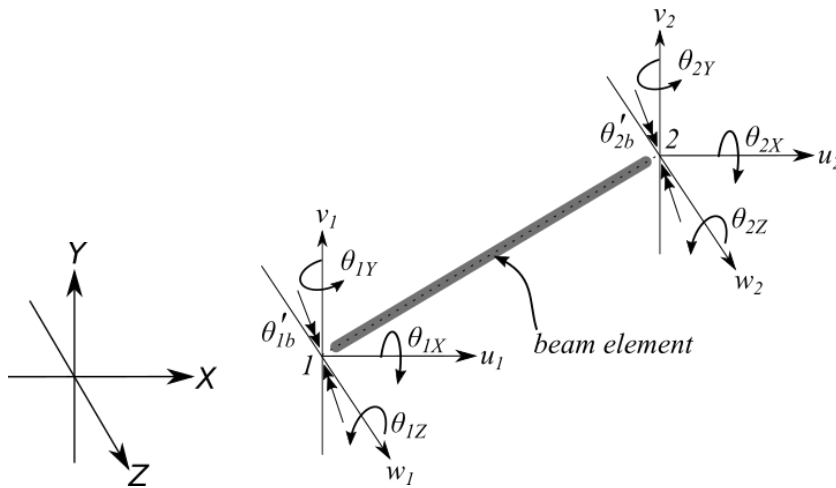
Figure 1 Global degree of freedom systems

The global end displacements are represented in vector form as

$$U = \begin{bmatrix} u_1 & v_1 & w_1 & \theta_{1X} & \theta_{1Y} & \theta_{1Z} & \theta_{1b}^{'} & u_2 & v_2 & w_2 & \theta_{2X} & \theta_{2Y} & \theta_{2Z} & \theta_{2b}^{'} \end{bmatrix}^T \qquad (1)$$

The corresponding global end actions are represented by

$$F = \begin{bmatrix} F_{1X} & F_{1Y} & F_{1Z} & M_{1X} & M_{1Y} & M_{1Z} & M_{1b}^{'} & F_{2X} & F_{2Y} & F_{2Z} & M_{2X} & M_{2Y} & M_{2Z} & M_{2b}^{'} \end{bmatrix}^T \qquad (2)$$

where M'_{1b} and M'_{2b} are the bimoments at the beam ends 1 and 2 respectively.

2.1.2 Local coordinate systems

In the co-rotational formulation, the rigid body components (translational DoFs) are removed from the element and only the axial, rotational and torsional components are retained in the local coordinate system. Hence, at the local level, the element has only 4 DoFs at each end: 3 rotations and 1 warping DoF, and an axial elongation within the element (Figure 2).
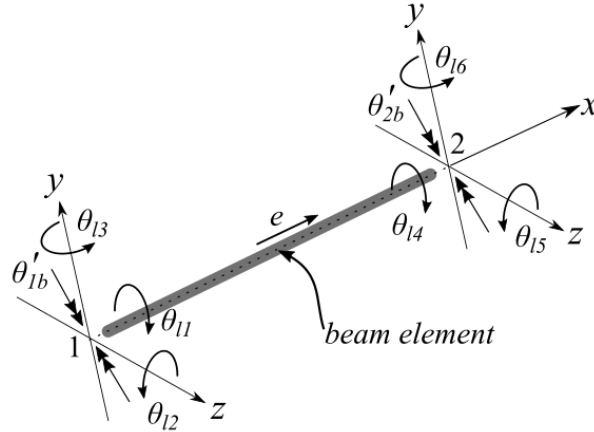
Figure 2 Local degree of freedom systems

The 9 local displacements are represented in vector form as

$$\boldsymbol{u} = \begin{bmatrix} \theta_{l1} & \theta_{l2} & \theta_{l3} & \theta'_{1b} & \theta_{l4} & \theta_{l5} & \theta_{l6} & \theta'_{2b} & e \end{bmatrix}^T \tag{3}$$

The corresponding local end actions are

$$\boldsymbol{f} = \begin{bmatrix} M_{l1} & M_{l2} & M_{l3} & M'_{1b} & M_{l4} & M_{l5} & M_{l6} & M'_{2b} & N_l \end{bmatrix}^T \tag{4}$$

In the above expressions, $\theta'_{1b}, \theta'_{2b}$ are the end twist; e is the axial deformation, M'_{1b} and M'_{2b} are the bimoments at each end. The other notations are self-explanatory. As noted in Figure 1 and Figure 2, the warping DoF remains constant during transformation from local system to global system as warping is in itself a deformational quantity and having effect only on the local element formulation [9].

2.2 Elastic Beam-Column Element

2.2.1 Elastic stiffness relations

The elastic beam-column element (EB) formulation within the co-rotational framework for the doubly-symmetric sections has been implemented in [8, 9]. The first order stiffness relations are developed by treating individual deformation and corresponding end actions in isolation based on the linear-elastic theory. The stiffness equation relating the end actions and deformation within the local coordinate systems is

$$\boldsymbol{f} = \boldsymbol{k}_l \boldsymbol{u} \tag{5}$$

where $\boldsymbol{f}$ is given by equation(4), $\boldsymbol{u}$ by equation(3) and $\boldsymbol{k}_l$ by

$$k_l = \begin{bmatrix} \frac{12EC_w}{L^3}+\frac{6GJ}{5L} & 0 & 0 & \frac{6EC_w}{L^2}+\frac{GJ}{10} & -\left(\frac{12EC_w}{L^3}+\frac{6GJ}{5L}\right) & 0 & 0 & \frac{6EC_w}{L^2}+\frac{GJ}{10} & 0 \\ 0 & \frac{4EI_z}{L} & 0 & 0 & 0 & \frac{2EI_z}{L} & 0 & 0 & 0 \\ 0 & 0 & \frac{4EI_y}{L} & 0 & 0 & 0 & \frac{2EI_y}{L} & 0 & 0 \\ \frac{6EC_w}{L^2}+\frac{GJ}{10} & 0 & 0 & \frac{4EC_w}{L}+\frac{2GJL}{15} & -\left(\frac{6EC_w}{L^2}+\frac{GJ}{10}\right) & 0 & 0 & \frac{2EC_w}{L}-\frac{GJL}{30} & 0 \\ -\left(\frac{12EC_w}{L^3}+\frac{6GJ}{5L}\right) & 0 & 0 & -\left(\frac{6EC_w}{L^2}+\frac{GJ}{10}\right) & \frac{12EC_w}{L^3}+\frac{6GJ}{5L} & 0 & 0 & -\left(\frac{6EC_w}{L^2}+\frac{GJ}{10}\right) & 0 \\ 0 & \frac{2EI_z}{L} & 0 & 0 & 0 & \frac{4EI_z}{L} & 0 & 0 & 0 \\ 0 & 0 & \frac{2EI_y}{L} & 0 & 0 & 0 & \frac{4EI_y}{L} & 0 & 0 \\ \frac{6EC_w}{L^2}+\frac{GJ}{10} & 0 & 0 & \frac{2EC_w}{L}-\frac{GJL}{30} & -\left(\frac{6EC_w}{L^2}+\frac{GJ}{10}\right) & 0 & 0 & \frac{4EC_w}{L}+\frac{2GJL}{15} & 0 \\ 0 & 0 & 0 & 0 & 0 & 0 & 0 & 0 & \frac{EA}{L} \end{bmatrix} \quad (6)$$

The basis and further details of the derivation can be found in [1, 2, 14].

The stiffness matrix k_l in equation (6) refers to the beam with coincident shear centre and centroid. For the open section beam with eccentric shear centre and centroid, the cross-section transformation derived in Section 2.4 is needed to be incorporated prior to the co-rotational transformation. Further, the torsional rigidity GJ is required to be modified for the general EB element to incorporate the Wagner terms, the details of which are provided in the following section.

As the EB element is developed on the basis of linear-elastic theory, non-linear geometric effects are ignored at the local element level[9]. However, they can be adequately captured during the co-rotational transformation from local to global systems provided sufficient number of elements are used along the beam member.

2.2.2 Modification of torsional rigidity

For the EB elements to predict the buckling load, the torsional rigidity GJ is required to be modified to include the Wagner effect[15, 16] as follows:

$$(GJ)_m = GJ + N(r_0^2 + y_0^2 + z_0^2) + \beta_y M_y + \beta_z M_z \quad (7)$$

where r_0 is given by:

$$r_0^2 = \frac{I_y + I_z}{A} \quad (8)$$

and β_y and β_z are the monosymmetry section constants in the respective directions given by:

$$\beta_y = \int_A z(y^2 + z^2)dA / I_y - 2z_0$$

$$\beta_z = \int_A y(y^2 + z^2)dA / I_z - 2y_0 \quad (9)$$

In the above, N is the axial force within the element and is negative for a beam-column in compression; and M_y and M_z are moments about the principal y-axis and z-axis respectively.

The theoretical basis of this equation can be traced to torsional buckling equations derived by Timonshenko [15] and energy equations by Trahair [16].

2.3 Displacement-based Beam-column Element

The displacement-based beam-column element (DB) is a higher order element compared to the elastic beam-column (EB) element. In the case of DB element, besides the inclusion of normal strains arising from the axial deformation, flexural deformation and warping, it also takes account of strain contributions arising from the coupling of stress resultants. One underpinning assumption for the DB element is that the strain developed within the element is considered to be small while undergoing large displacement and large rotations.

The DB element also possesses the capability to accommodate the spread of plasticity along the length and within the cross-section of the element. However, this capability is not tested in this research report. The stiffness relations for the DB element are discussed next.

2.3.1   Displacement field

Consider a case where a typical thin-walled open cross-section undergoes translation followed by the rotation about the shear centre axis (Figure 3). During this deformation process, the shear centre of the cross-section undergoes displacements u, v and w parallel to the original x,y, z axes, and twist rotation ϕ about the shear centre axis parallel to the x-axis. Hence the shear centre S translates to S_1 and the point P moves to P_1 and then finally to P_2 as a result of rotation about the longitudinal axis passing through S_1.
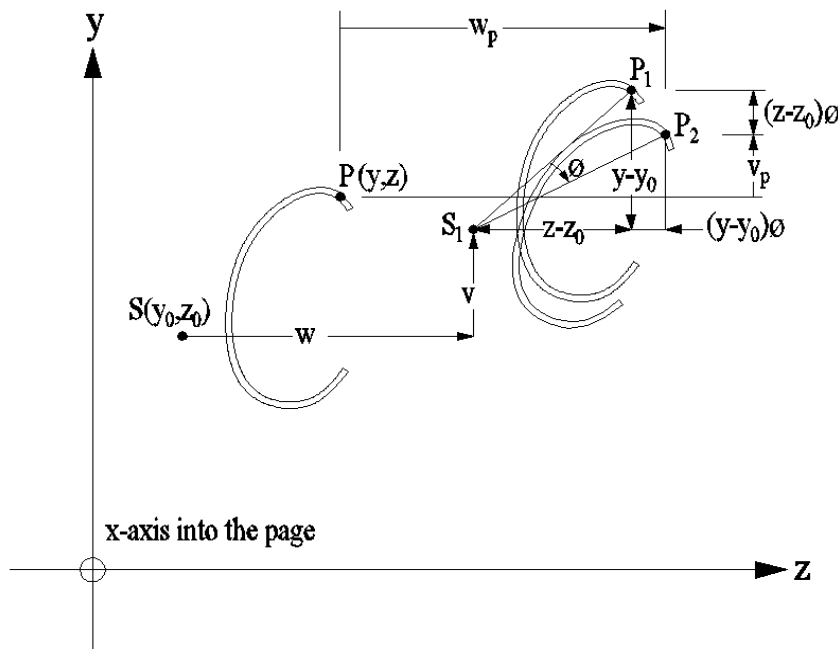
Figure 3 Displacements and rotations of arbitrary thin-walled open cross-section

The corresponding displacements (u_p, v_p, w_p) of a point $P(y,z)$ on the cross-section in the respective x, y and z direction are given by:

$$u_p = u - yv' - zw' + \omega\phi' - yw'\phi + zv'\phi$$

$$v_p = v - (z - z_0)\phi \tag{10}$$

$$w_p = w + (y - y_0)\phi$$

where (y_0, z_0) are the coordinates of the shear centre and ω is the normalized sectorial coordinate with respect to the shear centre. Similar derivation for a different axis system is provided in [16].

The sectorial coordinate (sectorial area) ω is defined as [15, 16, 17]:

$$\omega = \omega_0 - \int_0^s \rho_0 ds \tag{11}$$

where ρ_0 is the perpendicular distance from the shear centre to the tangent to the centreline of the cross-section and s is the distance along the centreline of the cross-section. The sign of ρ_0 is taken as positive in counter-clockwise direction. ω_0 is given by:

$$\omega_0 = \frac{1}{A}\int_A \left[\int_0^s \rho_0 ds \right] dA \tag{12}$$

The equation (11) satisfies the condition $\int_A \omega dA = 0$.

In the co-rotational formulation, the rigid body motion components of deformation are ignored. Hence, the transverse displacement (v, w) and torsional displacement (ϕ) are expressed in terms of end rotations. Likewise, axial displacement u is expressed in terms of normal elongation e for the whole length of beam. Hence, the displacement functions describing the deformations of beam-column element are given by:

$$u = N_{u1}e$$

$$v = N_{v1}\theta_{l2} + N_{v2}\theta_{l5}$$

$$w = N_{w1}\theta_{l3} + N_{w2}\theta_{l6} \tag{13}$$

$$\phi = N_{\phi 1}\theta_{l1} + N_{\phi 2}\theta_{1b}' + N_{\phi 3}\theta_{l4} + N_{\phi 4}\theta_{2b}'$$

where N_{u1}, N_{v1}, N_{v2}, N_{w1}, N_{w2}, $N_{\phi 1}$, $N_{\phi 2}$, $N_{\phi 3}$ and $N_{\phi 4}$ are respective shape functions given by [8, 14]:

$$N_{u1} = \frac{x}{L}$$

$$N_{v1} = N_{w1} = N_{\phi 2} = x\left(1 - \frac{x}{L}\right)^2$$

$$N_{v2} = N_{w2} = N_{\phi 4} = x\left(\frac{x}{L}\right)\left(\frac{x}{L} - 1\right) \tag{14}$$

$$N_{\phi 1} = 1 - 3\left(\frac{x}{L}\right)^2 + 2\left(\frac{x}{L}\right)^3$$

$$N_{\phi 3} = 3\left(\frac{x}{L}\right)^2 - 2\left(\frac{x}{L}\right)^3$$

The displacement functions and end DoFs can be expressed in matrix form as

$$
\begin{aligned}
u &= \boldsymbol{N}_u^T \boldsymbol{u} \\
v &= \boldsymbol{N}_v^T \boldsymbol{u} \\
w &= \boldsymbol{N}_w^T \boldsymbol{u} \\
\phi &= \boldsymbol{N}_\phi^T \boldsymbol{u}
\end{aligned}
\tag{15}
$$

where

$$
\begin{aligned}
\boldsymbol{N}_u^T &= \begin{bmatrix} 0 & 0 & 0 & 0 & 0 & 0 & 0 & 0 & N_{u1} \end{bmatrix} \\
\boldsymbol{N}_v^T &= \begin{bmatrix} 0 & N_{v1} & 0 & 0 & 0 & N_{v2} & 0 & 0 & 0 \end{bmatrix} \\
\boldsymbol{N}_w^T &= \begin{bmatrix} 0 & 0 & N_{w1} & 0 & 0 & 0 & N_{w2} & 0 & 0 \end{bmatrix} \\
\boldsymbol{N}_w^T &= \begin{bmatrix} N_{\phi1} & 0 & 0 & N_{\phi2} & N_{\phi3} & 0 & 0 & N_{\phi4} & 0 \end{bmatrix}
\end{aligned}
\tag{16}
$$

and $\boldsymbol{u}$ is given by equation(3).

2.3.2   Strain-displacement relation

For large displacement analysis, the longitudinal finite strain at the point P(y,z) on the cross-section is expressed as [3]:

$$
\varepsilon_p = \frac{\partial u_p}{\partial x} + \frac{1}{2}\left[\left(\frac{\partial u_p}{\partial x}\right)^2 + \left(\frac{\partial v_p}{\partial x}\right)^2 + \left(\frac{\partial w_p}{\partial x}\right)^2\right]
\tag{17}
$$

For small strains, this may be approximated by:

$$
\varepsilon_p = \frac{\partial u_p}{\partial x} + \frac{1}{2}\left[\left(\frac{\partial v_p}{\partial x}\right)^2 + \left(\frac{\partial w_p}{\partial x}\right)^2\right]
\tag{18}
$$

By substituting the corresponding derivatives of equation(10) into equation(18), the axial strain is obtained as:

$$
\begin{aligned}
\varepsilon_p ={}& u' - yv'' - zw'' + \omega\phi'' + \frac{1}{2}\left[(v')^2 + (w')^2\right] + \frac{1}{2}\left[(y - y_0)^2 + (z - z_0)^2\right](\phi')^2 \\
&+ (z_0 v' - y_0 w')\phi' + (zv'' - yw'')\phi
\end{aligned}
\tag{19}
$$

The shear strain γ_p at point P(y,z) due to uniform torsion is given by [3]:

$$
\gamma_p = 2n\kappa_z
\tag{20}
$$

where κ_z is the twist given by:

$$
\kappa_z = \phi' + \frac{1}{2}\left(v''w' - v'w''\right)
\tag{21}
$$

By assuming that twist due to bending is negligibly small, the shear strain due to uniform torsion can be approximated by:

$$\gamma_p = 2n\phi' \tag{22}$$

in which n is the perpendicular distance of point P(y,z) from the mid-thickness line of the cross-section. The axial strain ε_p and the shear strain γ_p can be put together in vector form as:

$$\varepsilon = \begin{bmatrix} \varepsilon_p \\ \gamma_p \end{bmatrix} \tag{23}$$

The terms in the strain vector can be expressed in matrix form as:

$$\varepsilon = Yd \tag{24}$$

where

$$Y = \begin{bmatrix} 1 & y & z & (y-y_0)^2 + (z-z_0)^2 & \omega & 0 \\ 0 & 0 & 0 & 0 & 0 & 2n \end{bmatrix} \tag{25}$$

and

$$d = \begin{bmatrix} u' + \dfrac{1}{2}\left[(v')^2 + (w')^2\right] + (z_0 v' - y_0 w')\phi' \\ -v'' - w''\phi \\ -w'' + v''\phi \\ \dfrac{1}{2}(\phi')^2 \\ \phi'' \\ \phi' \end{bmatrix} \tag{26}$$

The variation of strain vector ε is obtained as:

$$\delta\varepsilon = Y\delta d \tag{27}$$

in which

$$\delta d = \begin{bmatrix} \delta\varepsilon_x \\ \delta\kappa_z \\ \delta\kappa_y \\ \delta\kappa_W \\ \delta\kappa_x \\ \delta\phi' \end{bmatrix} = \begin{bmatrix} \delta u' \\ -\delta v'' \\ -\delta w'' \\ 0 \\ \delta\phi'' \\ \delta\phi' \end{bmatrix} + \begin{bmatrix} v'\delta v' + w'\delta w' - y_0(w'\delta\phi' + \phi'\delta w') + z_0(v'\delta\phi' + \phi'\delta v') \\ -\phi\,\delta w'' - w''\delta\phi \\ +\phi\delta v'' + v''\delta\phi \\ \phi'\,\delta\phi' \\ 0 \\ 0 \end{bmatrix} \tag{28}$$

δd can be expressed as

$$\delta d = N_{\delta d1}\delta v \tag{29}$$

where

$$
N_{\delta d1} = \begin{bmatrix}
1 & v'+z_0\phi' & w'-y_0\phi' & 0 & 0 & 0 & z_0 v'-y_0 w' & 0 \\
0 & 0 & 0 & -1 & -\phi & -w'' & 0 & 0 \\
0 & 0 & 0 & +\phi & -1 & +v'' & 0 & 0 \\
0 & 0 & 0 & 0 & 0 & 0 & \phi' & 0 \\
0 & 0 & 0 & 0 & 0 & 0 & 0 & 1 \\
0 & 0 & 0 & 0 & 0 & 0 & 1 & 0
\end{bmatrix}
\tag{30}
$$

$$
\delta v = \begin{bmatrix} \delta u' & \delta v' & \delta w' & \delta v'' & \delta w'' & \delta\phi & \delta\phi' & \delta\phi'' \end{bmatrix}^T
\tag{31}
$$

Using equations (13) to (15) and taking variation of them, yields

$$
\delta v = N_{\delta d2}\delta u
\tag{32}
$$

where

$$
N_{\delta d2} = \begin{bmatrix}
0 & 0 & 0 & 0 & 0 & 0 & 0 & 0 & N_{u1}' \\
0 & N_{v1}' & 0 & 0 & 0 & N_{v2}' & 0 & 0 & 0 \\
0 & 0 & N_{w1}' & 0 & 0 & 0 & N_{w2}' & 0 & 0 \\
0 & N_{v1}' & 0 & 0 & 0 & N_{v2}' & 0 & 0 & 0 \\
0 & 0 & N_{w1}' & 0 & 0 & 0 & N_{w2}' & 0 & 0 \\
N_{\phi1} & 0 & 0 & N_{\phi2} & N_{\phi3} & 0 & 0 & N_{\phi4} & 0 \\
N_{\phi1}' & 0 & 0 & N_{\phi2}' & N_{\phi3}' & 0 & 0 & N_{\phi4}' & 0 \\
N_{\phi1}'' & 0 & 0 & N_{\phi2}'' & N_{\phi3}'' & 0 & 0 & N_{\phi4}'' & 0
\end{bmatrix}
\tag{33}
$$

and u is the DoFs at the two ends of the element given by equation (3).

Finally, the variation of normal strain can be finally expressed as:

$$
\delta\varepsilon = Y N_{\delta d1} N_{\delta d2}\delta u
\tag{34}
$$

where Y is given by equation (25), $N_{\delta d1}$ by (30) and $N_{\delta d2}$ by (33). The variational form of longitudinal strain is used for the determination of elastic stiffness matrix in Section 2.3.4.

2.3.3   Stress-strain relations

The stresses and the corresponding strains at the point P(y,z) on the cross-section are related by

$$
\sigma = D\varepsilon
\tag{35}
$$

and the corresponding variation of stress vector is

$$
\delta\sigma = D\delta\varepsilon
\tag{36}
$$

in which

$$\boldsymbol{\sigma} = \begin{bmatrix} \sigma_p \\ \tau_p \end{bmatrix} \quad \text{and} \quad \boldsymbol{D} = \begin{bmatrix} E & 0 \\ 0 & G \end{bmatrix} \tag{37}$$

and strain vector $\boldsymbol{\varepsilon}$ is given by equation (23). *E* and *G* are elastic modulus and shear modulus respectively. They are related through

$$G = \frac{E}{2(1+\nu)} \tag{38}$$

where ν is the Poisson's ratio.

2.3.4 Elastic stiffness matrix

For a structure to be in equilibrium under deformed configuration, the principle of virtual work requires that internal virtual work due to straining of the structure must be equal to the external virtual work due to external forces on the structures.

Mathematically, it requires that

$$\delta W_i - \delta W_e = 0 \tag{39}$$

where $\delta \boldsymbol{W_i}$ is the internal virtual work and $\delta \boldsymbol{W_e}$ is the external virtual work.

The variation of virtual work equation (39) defines the stability of structures[16]. For neutral equilibrium (buckling),

$$\delta^2 \boldsymbol{W}_i - \delta^2 \boldsymbol{W}_e = 0 \tag{40}$$

for any sets of virtual deformation δu, δv, δw, $\delta \phi$.

Now, for a beam element, the internal virtual work is given by:

$$\delta W_i = \int_{V_0} \delta \boldsymbol{\varepsilon}^T \boldsymbol{\sigma} dV \tag{41}$$

and external virtual work by:

$$\delta W_e = \delta \boldsymbol{u}^T \boldsymbol{Q}_{ext} \tag{42}$$

Using equation(34), internal virtual work, $\delta \boldsymbol{W_i}$ can be expressed as

$$\begin{aligned}
\delta W_i &= \delta \boldsymbol{u}^T \int_{l_0} \boldsymbol{N}_{\delta d2}^T \boldsymbol{N}_{\delta d1}^T \left(\int_A \boldsymbol{Y}^T \boldsymbol{\sigma} dA \right) dx \\
&= \delta \boldsymbol{u}^T \int_{l_0} \boldsymbol{N}_{\delta d2}^T \boldsymbol{N}_{\delta d1}^T \boldsymbol{S}_f dx
\end{aligned} \tag{43}$$

Using equation (39), we get

$$\delta \boldsymbol{u}^T \left[\int_{l_0} \boldsymbol{N}_{\delta d2}^T \boldsymbol{N}_{\delta d1}^T \boldsymbol{S}_f dx - \boldsymbol{Q}_{ext} \right] = 0 \quad or \quad \boldsymbol{q}_{int} - \boldsymbol{Q}_{ext} = 0 \tag{44}$$

where internal force vector $\boldsymbol{q}_{\text{int}}$ is:

$$\boldsymbol{q}_{\text{int}} = \int_{l_0} \boldsymbol{N}_{\delta d2}^T \boldsymbol{N}_{\delta d1}^T \boldsymbol{S}_f \, dx \tag{45}$$

$\boldsymbol{S}_f$ is the vector of section force (stress resultants) expressed as

$$\boldsymbol{S}_f = \int_{A_0} \boldsymbol{Y}^T \boldsymbol{\sigma} \, dA$$

$$= \int_{A_0} \begin{bmatrix} 1 & 0 \\ y & 0 \\ z & 0 \\ (y-y_0)^2 + (z-z_0)^2 & 0 \\ \omega & 0 \\ 0 & 2n \end{bmatrix} \begin{bmatrix} \sigma \\ \tau \end{bmatrix} dA = \begin{bmatrix} \int_{A_0} \sigma \, dA \\ \int_{A_0} y\sigma \, dA \\ \int_{A_0} z\sigma \, dA \\ \int_{A_0} \left[(y-y_0)^2 + (z-z_0)^2 \right] \sigma \, dA \\ \int_{A_0} \omega\sigma \, dA \\ \int_{A_0} 2n\tau \, dA \end{bmatrix} \tag{46}$$

whereby,

$$N = \int_{A_0} \sigma \, dA$$

$$-M_z = \int_{A_0} y\sigma \, dA$$

$$M_y = \int_{A_0} z\sigma \, dA$$

$$W_0 = \int_{A_0} \left[(y-y_0)^2 + (z-z_0)^2 \right] \sigma \, dA \tag{47}$$

$$B = \int_{A_0} \omega\sigma \, dA$$

$$T = \int_{A_0} 2n\tau \, dA$$

in which *N, M_z ,M_y ,W_0, B* and *T* are axial force, bending moment about the z-axis, bending moment about the y-axis, Wagner stress resultant, bimoment and uniform torque at the particular cross-section of the beam.

Using equation(40), the elastic stiffness matrix for a displacement-based beam-column element can be obtained as

$$\delta^2 W_i = \int_{V_0} \delta^2 \boldsymbol{\varepsilon}^T \boldsymbol{\sigma} \, dV + \int_{V_0} \delta \boldsymbol{\varepsilon}^T \delta \boldsymbol{\sigma} \, dV \tag{48}$$

Substituting equations (36) and (43) into (48), we get

$$\delta^2 W_i = \delta \boldsymbol{u}^T \int_{l_0} \boldsymbol{N}_{\delta d2}^T \delta \boldsymbol{N}_{\delta d1}^T \boldsymbol{S}_f dx + \int_{V_0} \delta \boldsymbol{\varepsilon}^T \boldsymbol{D} \delta \boldsymbol{\varepsilon} dV \qquad (49)$$

The product of $\delta \boldsymbol{N}_{\delta d1}$ and $\boldsymbol{S}_f$ can be further expressed as

$$\delta \boldsymbol{N}_{\delta d1}^T \boldsymbol{S}_f = \boldsymbol{G} \boldsymbol{N}_{\delta d2} \delta \boldsymbol{u} \qquad (50)$$

where $\boldsymbol{G}$ in first part of equation (49) is the stability matrix at the local level given by:

$$\boldsymbol{G} = \begin{bmatrix} 0 & 0 & 0 & 0 & 0 & 0 & 0 & 0 \\ 0 & N & 0 & 0 & 0 & 0 & Nz_0 & 0 \\ 0 & 0 & N & 0 & 0 & 0 & -Ny_0 & 0 \\ 0 & 0 & 0 & 0 & 0 & M_y & 0 & 0 \\ 0 & 0 & 0 & 0 & 0 & M_z & 0 & 0 \\ 0 & 0 & 0 & M_y & M_z & 0 & 0 & 0 \\ 0 & Nz_0 & -Ny_0 & 0 & 0 & 0 & W_0 & 0 \\ 0 & 0 & 0 & 0 & 0 & 0 & 0 & 0 \end{bmatrix} \qquad (51)$$

Hence, substituting the relevant expressions into the equation(49), we have

$$\delta^2 W_i = \delta \boldsymbol{u}^T \left[\int_{l_0} \boldsymbol{N}_{\delta d2}^T \boldsymbol{G} \boldsymbol{N}_{\delta d2} dx + \int_{l_0} \boldsymbol{N}_{\delta d2}^T \boldsymbol{N}_{\delta d1}^T \left(\int_{A_0} \boldsymbol{Y}^T \boldsymbol{D} \boldsymbol{Y} dA \right) \boldsymbol{N}_{\delta d1} \boldsymbol{N}_{\delta d2} dx \right] \delta \boldsymbol{u} \qquad (52)$$

where the terms within the square bracket represent the elastic stiffness matrix in the local coordinate system.

Thus,

$$\boldsymbol{k}_l = \int_{l_0} \boldsymbol{N}_{\delta d2}^T \boldsymbol{G} \boldsymbol{N}_{\delta d2} dx + \int_{l_0} \boldsymbol{N}_{\delta d2}^T \boldsymbol{N}_{\delta d1}^T \boldsymbol{k}_t \boldsymbol{N}_{\delta d1} \boldsymbol{N}_{\delta d2} dx \qquad (53)$$

where $\boldsymbol{k}_t$ is the elastic section tangent stiffness matrix given by:

$$\boldsymbol{k}_t = \int_{A_0} \boldsymbol{Y}^T \boldsymbol{D} \boldsymbol{Y} dA \qquad (54)$$

Upon substituting $\boldsymbol{Y}$ from equation (25) and $\boldsymbol{D}$ from equation(37), $\boldsymbol{k}_t$ is obtained as

$$\boldsymbol{k}_t = \int_{A_0} E \begin{bmatrix} 1 & y & z & p^2 & \omega & 0 \\ y & y^2 & yz & p^2 y & \omega y & 0 \\ z & yz & z^2 & p^2 z & \omega z & 0 \\ p^2 & p^2 y & p^2 z & p^4 & p^2 \omega & 0 \\ \omega & \omega y & \omega z & p^2 \omega & \omega^2 & 0 \\ 0 & 0 & 0 & 0 & 0 & G(4n^2)/E \end{bmatrix} dA \qquad (55)$$

in which $p^2 = (y - y_0)^2 + (z - z_0)^2$.

The element stiffness matrix given by equation (53) for the displacement-based beam-column element are further required to be modified to account for non-coincident location of shear centre and centroid as is the case in mono-symmetric and asymmetric sections. The details of the transformation required to account for this change are described next.

2.4 Transformation of element stiffness matrix for general sections

The stiffness relations of equation (5) are derived for beam-column elements with coincident shear centre and centroid. Further, the stiffness relations described in section 2.3.4 assumes that force systems relate to the shear centre. Since the thin-walled sections such as single channel sections have eccentric shear centre and centroid, the above stiffness relations are not directly applicable but required to be transformed prior to the application of co-rotational transformation.

Within the framework of conventional thin-walled beam-column element formulation, there are seven actions with corresponding displacements at each end of a thin-walled beam element. These include three forces (F_x, F_y, F_z), three moments (M_x, M_y, M_z) and one bimoment ($M_b^{'}$). In the case of thin-walled beam elements, they do not necessarily act through a common point [2]. The shear forces (F_y, F_z) act through the shear centre with directions parallel to the principal axes, the axial force (F_x) acts along the centroidal axis, the moments (M_y, M_z) act about the principal axes (y,z) but in planes containing the shear centre, and the torque (M_x) acts about the shear centre axis.

In conformation to the principles of co-rotational framework, the rigid body motion parts of the end actions are ignored and only the deformational parts are considered at the local level. Hence, the shear forces (F_y, F_z) are neglected and the axial force (F_x) at two ends are replaced by a single axial force, N within the element. This axial force, N acts through the centroid resulting in uniform axial deformation of the cross-section.

2.4.1   Transformation Matrix

In the following, a local transformation matrix is derived that relates the state of force system with axial force N acting at the shear centre (Figure 4) and at the centroid (Figure 5).

Note the absence of shear forces (F_y, F_z) from the two figures as befitting to the co-rotational approach of beam element formulation. These forces are however recovered at the global level through co-rotational transformation.
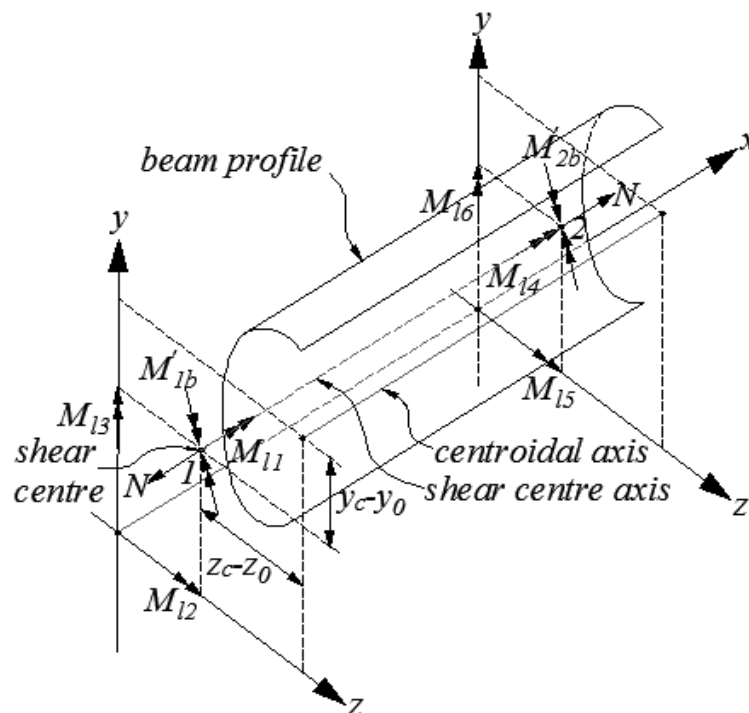
Figure 4 Element force system with axial force acting at the shear centre
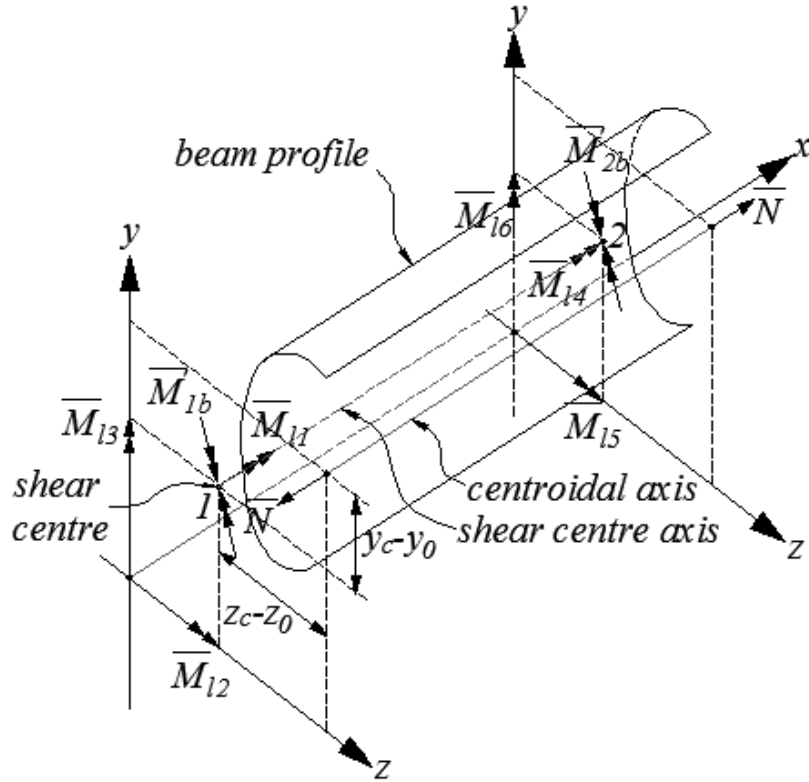
Figure 5 Element force system with axial force acting at the centroid

Due to the change in position of the axial force to the centroid, the moments and the bimoments are affected in the original force system. The new end actions are related to the original end actions as follow:

$$\bar{M}_{l1} = M_{l1}$$
$$\bar{M}_{l2} = M_{l2} - N(y_c - y_0)$$
$$\bar{M}_{l3} = M_{l3} + N(z_c - z_0)$$
$$\bar{M}_{1b}^{'} = M_{1b}^{'} + N\omega_c$$
$$\bar{M}_{l4} = M_{l4} \qquad\qquad (56)$$
$$\bar{M}_{l5} = M_{l5} + N(y_c - y_0)$$
$$\bar{M}_{l6} = M_{l6} - N(z_c - z_0)$$
$$\bar{M}_{2b}^{'} = M_{2b}^{'} - N\omega_c$$
$$\bar{N} = N$$

where ω_c is the sectorial coordinate at the point of application of concentrated axial force, here in this case is the centroid. However, if the axial force is applied as a uniform stress, this terms is not considered.

The above set of equations can be arranged in matrix format as

$$\bar{f} = Af \qquad\qquad (57)$$

where

$$\overline{f} = \left[\overline{M}_{l1}, \overline{M}_{l2}, \overline{M}_{l3}, \overline{M}'_{1b}, \overline{M}_{l4}, \overline{M}_{l5}, \overline{M}_{l6}, \overline{M}'_{2b}, \overline{N} \right]^T \tag{58}$$

$$f = \left[M_{l1}, M_{l2}, M_{l3}, M'_{1b}, M_{l4}, M_{l5}, M_{l6}, M'_{2b}, N \right]^T \tag{59}$$

and

$$A = \begin{bmatrix} 1 & 0 & 0 & 0 & 0 & 0 & 0 & 0 & 0 \\ 0 & 1 & 0 & 0 & 0 & 0 & 0 & 0 & -(y_c - y_0) \\ 0 & 0 & 1 & 0 & 0 & 0 & 0 & 0 & +(z_c - z_0) \\ 0 & 0 & 0 & 1 & 0 & 0 & 0 & 0 & \omega_c \\ 0 & 0 & 0 & 0 & 1 & 0 & 0 & 0 & 0 \\ 0 & 0 & 0 & 0 & 0 & 1 & 0 & 0 & +(y_c - y_0) \\ 0 & 0 & 0 & 0 & 0 & 0 & 1 & 0 & -(z_c - z_0) \\ 0 & 0 & 0 & 0 & 0 & 0 & 0 & 1 & -\omega_c \\ 0 & 0 & 0 & 0 & 0 & 0 & 0 & 0 & 1 \end{bmatrix} \tag{60}$$

in which $\overline{f}$ is the force system in the transformed coordinates, f is the force system in the original coordinates, and A is the transformation matrix resulting from the translation of axial force from shear centre to centroid of the cross-section. Based on the reciprocal theorem, it can be concluded that the nodal degrees of freedom after the transformation of axial force to the centroid is

$$u = A^T \overline{u} \tag{61}$$

Utilizing equations(57) and (61), the transformed local stiffness matrix can be expressed as

$$\overline{k}_l = A k_l A^T \tag{62}$$

2.5 Global stiffness matrix

Within the co-rotational framework, the relation between the local and the global variables is obtained [12] as

$$\delta \overline{u} = T \delta U \tag{63}$$

and from the principle of virtual work, the work conjugate relationship between the local frame and the global frame can be expressed as

$$\delta \overline{u}^T \overline{f} = \delta U^T F \tag{64}$$

Substitution of equation (63) into equation (64) yields

$$F = T^T \overline{f} \tag{65}$$

which relates the force system in the global coordinates to the local transformed coordinates. The global stiffness relation can be obtained by taking the derivative of equation (65) as

$$\delta \boldsymbol{F} = \delta \boldsymbol{T}^T \overline{\boldsymbol{f}} + \boldsymbol{T}^T \delta \overline{\boldsymbol{f}}$$
$$= \delta \boldsymbol{T}^T \boldsymbol{A}\boldsymbol{f} + (\boldsymbol{T}^T \boldsymbol{A}\boldsymbol{k}_l \boldsymbol{A}^T \boldsymbol{T})\delta \boldsymbol{U} \qquad (66)$$
$$= (\boldsymbol{K}_\sigma + \boldsymbol{K})\delta \boldsymbol{U}$$

where $\boldsymbol{K}_\sigma$ is the geometric stiffness matrix and $\boldsymbol{K}$ is the tangent stiffness matrix in the global coordinate systems. $\boldsymbol{K}_\sigma$ accounts for the large displacement effects [12]. Thus the global stiffness relation in the co-rotational frame is achieved through the co-rotational transformation matrix $\boldsymbol{T}$ which has warping degree of freedom included by Zhang [9]. The details of the derivation of geometric matrix $\boldsymbol{K}_\sigma$ is given in [12] whereas the tangent stiffness matrix $\boldsymbol{K}$ is provided herein in this report.

3. ADAPTION OF BEAM-COLUMN ELEMENTS IN OPENSEES

3.1 OpenSees Framework

An OpenSees (*Open System for Earthquake Engineering Simulation*) is an open-source finite element software framework that was developed by Pacific Earthquake Engineering Research Center [10]. It is designed to solve problems mainly in the field of structural and geotechnical systems. Within the structural framework, one of the key features of OpenSees is its capability to solve large displacement analysis of structures which is achieved through the co-rotational transformation integrated within its framework.

OpenSees is basically developed in object-oriented style. It is designed in modular form with loose coupling among modules [10]. This allows users and developers in different areas to develop and modify specific modules to build finite element applications with relatively little dependence on other modules. The finite element analysis itself is performed by integrating each module through the scripting language called Tool Command Language (TCL). Hence, TCL programming language forms the integral part of successful finite element modelling and analysis in OpenSees,

3.2 Modification to Beam-column Elements

The formulation for the elastic beam-column element (EB) and the displacement-based beam-column (DB) element for the non-symmetric sections are incorporated through the modification of three files in OpenSees: ElasticBeam3d, DispBeamColumn3d and FiberSection3d. Minor modifications are carried out in other interface files as well.

3.2.1 Elastic beam-column elements

The elastic beam element, that was previously modified to analyse the doubly symmetric thin-walled section [9], was further modified to take account of the general non-symmetric section. Here, the cross-section transformation matrix given by equation(60) is incorporated in the local stiffness relations. Torsional rigidity terms *GJ* in the stiffness matrix (equation(6)) was replaced by the equation (7) wherein internal axial force and moments were used to compute the modified torsional rigidity $(GJ)_m$.

3.2.2 Displacement-based beam-column elements

The incorporation of displacement based beam element in OpenSees requires that the section be discretised into several fibers with each fiber characterized by centroid, area, material and sectorial coordinate. For the typical channel cross-section (Figure 6), round corners were represented by 4 fibers, but for flat portions, the required number of fiber is determined such that the further increase in number of fibers does not result in significant deviation of results from the previous one. Since the

cold-formed thin-walled sections are often very thin, only one layer of fiber is used through the thickness of the section.

The inclusion of warping in the formulation requires that the normalized sectorial coordinate be computed at the centroid of each fiber. Unlike the doubly symmetric sections where the expression for sectorial coordinates is simple in form and can be readily integrated with little or no effort within the main file, the computation of sectorial properties in non-symmetric or mono-symmetric sections becomes more elaborate and engaging.

To address this problem, a separate function has been written in TCL language to automate the calculation of section properties including the normalized sectorial coordinates for any open section based on the theory outlined in [18,19] and numerical evaluation scheme outlined in [20]. A function was also written to discretise cross-section into fibers based on the given dimensions and its shape. The normalized sectorial coordinates along with the area, the material type and the centroid are then assigned to the fiber objects.
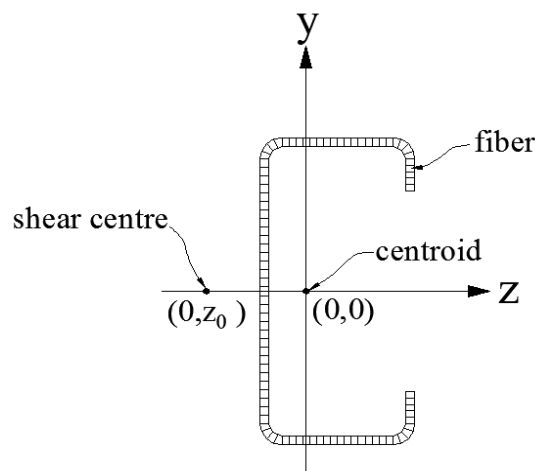
Figure 6 Fiber representation of channel section

For the program to work for general sections, it requires the input of shear centre coordinates to the fiber section object. This has been accomplished through the introduction of virtual function within the UniaxialFiber3d.h file in OpenSees framework.

Since the section forces (equation(46)) at the particular section along the beam is the aggregate of forces in individual fibers, it is represented by

$$
S_f = \begin{bmatrix} \displaystyle\sum_{i=1}^{r} \sigma_i A_i \\ \displaystyle\sum_{i=1}^{r} y_i \sigma_i A_i \\ \displaystyle\sum_{i=1}^{r} z_i \sigma_i A_i \\ \displaystyle\sum_{i=1}^{r} \left[(y_i - y_0)^2 + (z_i - z_0)^2 \right] \sigma_i A_i \\ \displaystyle\sum_{i=1}^{r} \omega_i \sigma_i A_i \\ \displaystyle\sum_{i=1}^{r} 2n\tau_i A_i \end{bmatrix} \tag{67}
$$

Where *r* refers to the number of fibers, σ_i is the stress, A_i is the area, ω_i is the sectorial coordinate, τ_i is the shear stress, and (y_i, z_i) is the coordinate of centroid of ith fiber on the cross-section.

Similarly, the elastic section tangent stiffness matrix in (55) is represented by

$$
\boldsymbol{k}_t = E \begin{bmatrix}
\sum_{i=1}^{r} A_i & \sum_{i=1}^{r} y_i A_i & \sum_{i=1}^{r} z_i A_i & \sum_{i=1}^{r} p_i^2 A_i & \sum_{i=1}^{r} \omega_i A_i & 0 \\
\sum_{i=1}^{r} y_i A_i & \sum_{i=1}^{r} y_i^2 A_i & \sum_{i=1}^{r} y_i z_i A_i & \sum_{i=1}^{r} p_i^2 y_i A_i & \sum_{i=1}^{r} \omega_i y_i A_i & 0 \\
\sum_{i=1}^{r} z_i A_i & \sum_{i=1}^{r} y_i z_i A_i & \sum_{i=1}^{r} z_i^2 A_i & \sum_{i=1}^{r} p_i^2 z_i A_i & \sum_{i=1}^{r} \omega_i z_i A_i & 0 \\
\sum_{i=1}^{r} p_i^2 A_i & \sum_{i=1}^{r} p_i^2 y_i A_i & \sum_{i=1}^{r} p_i^2 z_i A_i & \sum_{i=1}^{r} p_i^4 A_i & \sum_{i=1}^{r} p_i^2 \omega_i A_i & 0 \\
\sum_{i=1}^{r} \omega_i A_i & \sum_{i=1}^{r} \omega_i y_i A_i & \sum_{i=1}^{r} \omega_i z_i A_i & \sum_{i=1}^{r} p_i^2 \omega_i A_i & \sum_{i=1}^{r} \omega_i^2 A_i & 0 \\
0 & 0 & 0 & 0 & 0 & GJ/E
\end{bmatrix}
\tag{68}
$$

Where $p_i^2 = (y_i - y_0)^2 + (z_i - z_0)^2$ and other terms are defined in relevant sections. The section forces and stiffness are aggregated along the beam element using Gauss-Lobatto Integration scheme that is incorporated in the OpenSees.

The above two equations along with the other relevant equations and the section transformation matrix are incorporated in the OpenSees files namely displacementColumn3d.cpp and FiberSection3d.cpp that were previously modified for solving doubly-symmetric sections in [9].

By separating the determination of fiber properties from the main file, the program is able to achieve its generality. With the inclusion of function for the calculation of section properties, seamless integration has been achieved between the TCL input file and the main program. The program can further be adapted to analyze closed thin-walled sections provided sectorial coordinates for closed sections are furnished. Furthermore, slight tweaking of the TCL input file can accommodate multi-layer fiber through the thickness. This has, however, been found unnecessary for the thin-walled sections, especially the cold-formed steel sections.

3.3 Module Interaction and Analysis Process

The overall solution strategy for the nonlinear displacement based beam column elements are provided in [9] and the interaction of different objects in OpenSees during the analysis are detailed in [10]. As such no additional information is provided herein.

4. NUMERICAL EXAMPLES

In this section, the post-buckling behaviour of thin-walled beams and columns with open cross-sections are presented. The solutions are obtained from the OpenSees program that was modified to include the elastic beam-column element (EB) and displacement-based beam-column element (DB) developed in this report. The solutions obtained from the OpenSees program are verified using the widely-used finite element software ABAQUS [21]. For the purpose of numerical analysis, unless otherwise specifically mentioned, three sections shown in Figure 7, each representative of doubly symmetric, monosymmetric and asymmetric sections are used. The dimensions and the corresponding section properties are given below.

(a) I Section   (b) Channel Section   (c) Asymmetric Section
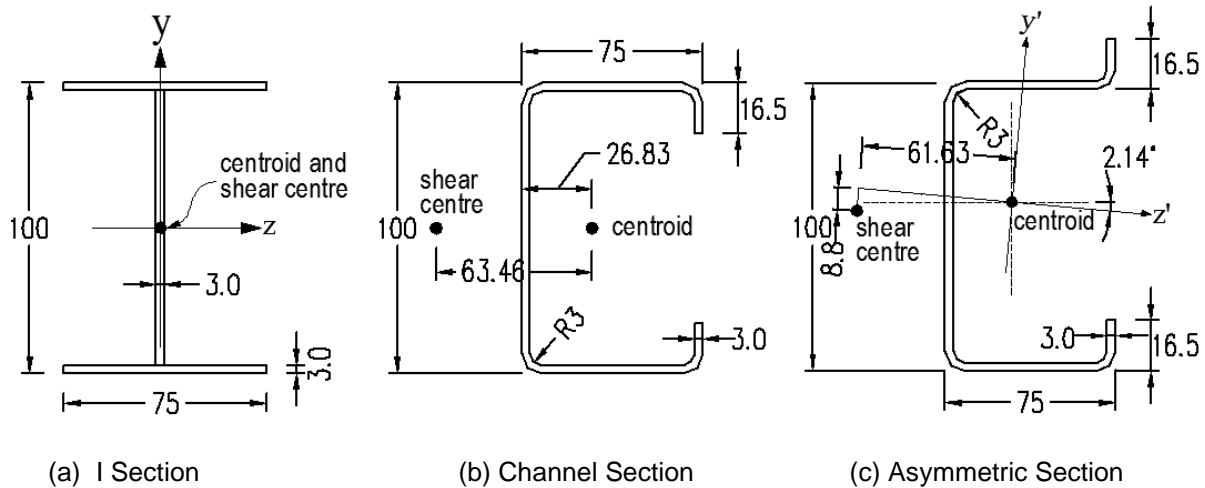
Figure 7 Dimensions for I, channel and asymmetric sections (in mm)

Table 1 Section Properties*

Properties	Units	I-Section	Channel Section	Asymmetric Section
A	mm^2	741.00	789.28	789.28
$I_{y'}$	mm^4	2.11×10^5	5.82×10^5	5.81×10^5
$I_{z'}$	mm^4	12.87×10^5	13.40×10^5	14.07×10^5
I_ω	mm^6	4.96×10^8	12.60×10^8	9.81×10^8
J	mm^4	2223.0	2367.84	2367.84
(y_0, z_0)	mm	(0,0)	(0,-63.46)	(-8.80,-61.63)
β_z	mm	0	0	19.65
β_y	mm	0	155.81	157.12
α	degree	0°	0°	-2.145°

*based on thin-walled theory

The elastic modulus, *E* is assumed as 2×10^5 and Poisson's ratio, ν as 0.3. The shear modulus *G* has been calculated using equation(38). In all the examples to follow, the linear-elastic material behaviour is assumed.

4.1 Doubly-symmetric Sections

4.1.1 I-section column subjected to compression

A simply supported 6m long I-section column is analysed for the post-buckling behaviour when subjected to compressive loads at the ends. The cross-section of the column is shown in Figure 7a. At either ends, the column is restrained against transverse displacement and x-axis rotation while allowing it to freely displace in the axial direction, rotate about y- and z-axis, and warp. It is however restrained against axial displacement at mid-length. Both the physical and analytical models are shown in Figure 8.

First the column is analysed for torsional buckling under compression. The buckling path is obtained based on a two-step process of analysis. In the first step, linear static analysis is carried out with small twisting moment (485 Nmm) acting about the longitudinal axis at the midspan. [This magnitude of twisting moment was arrived at based on the minimum lateral force at flange-web junctions required to twist the shell model as explained in the paragraphs to follow]. This introduces the twist deformation which ensures that the column buckles in torsional mode during the subsequent nonlinear analysis. It is necessary that the magnitude of this perturbation load must be sufficiently

small so that it does not affect the post-buckling solution but at the same time it must be large enough to trigger the deformation so that structures undergoes expected buckling modes [21].

(a) Physical Model   (b) Analytical Model
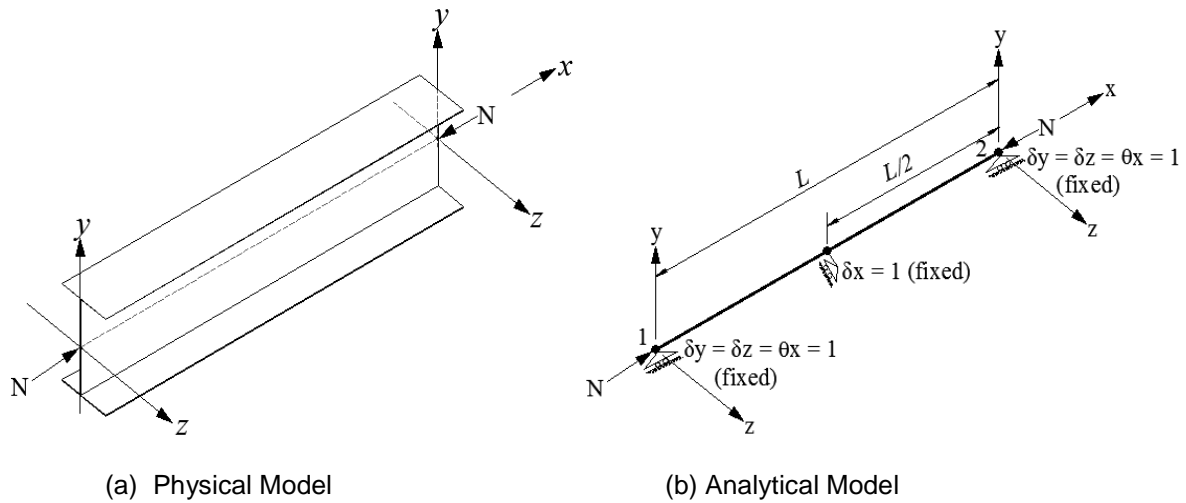
Figure 8 I-section column subjected to compressive load

In the second step, nonlinear analysis is carried out with reference compressive load, slightly exceeding the elastic buckling load, being applied at both ends. The nonlinear analysis is performed using the incremental-iterative force-controlled procedure. The problem is solved using the elastic beam-column element (EB) and the displacement-based beam-column element (DB). The post-buckling paths predicted by the DB elements are compared with the results obtained from the Abaqus nonlinear beam element (B32OS) and shell element (S8R). B32OS is a three-dimensional second-order(quadratic) beam elements which incorporates warping theory [21] and is specifically designed to analyse thin-walled open-sections. Likewise, S8R is a second-order eight-node doubly curved thick shell with reduced integration.

The load-deformation responses obtained from the OpenSees using different number of elements ((4 DB, 10 DB, 20 DB) along with the deformation-responses of Abaqus B32OS beam and S8R shell models are shown in Figure 9. In the figure, the number of elements used for each model is identified by the number before the element type within the legend. Although the EB element could accurately predict the buckling load, it was not able to produce the post-buckling path beyond the certain displacement range due to numerical instability after attaining the buckling load. Hence, the plot corresponding to EB element is not presented. However, it has been observed that the limited range of post-buckling path traced by EB element coincided with that of Abaqus B32OS beam element.

For the Abaqus S8R shell model, the boundary conditions at the supports were modelled by creating three small areas each on the centre of web and the flange-web junctions where they intersect with coordinate axes and assigning rigid body constraints to them. The actual boundary conditions were applied to the reference point on the rigid body regions instead of applying to the entire cross-section.

Since it was not possible to apply the twist moment directly to the shell model to introduce initial imperfection, it was simulated by applying a lateral force of magnitude 5N to the nodes located at the top and bottom flange-web junctions normal to the longitudinal axis of the column. The lateral forces were allowed to follow the nodal rotations so that they always remain tangent to the flange surface during the deformation process. The reference compressive loads were applied as the shell edge load on the cross-section at the ends. The nonlinear analysis was carried out using Riks method.

The discretization of S8R shell model consisted of 3600 elements with 300 elements along the column length, 4 elements on each flanges and 4 elements on the web. This does not include the small finite elements generated due to partitioning of model which is required for creating rigid body

area to apply boundary conditions. However, these small elements are found to have negligible impact on the solution accuracy.
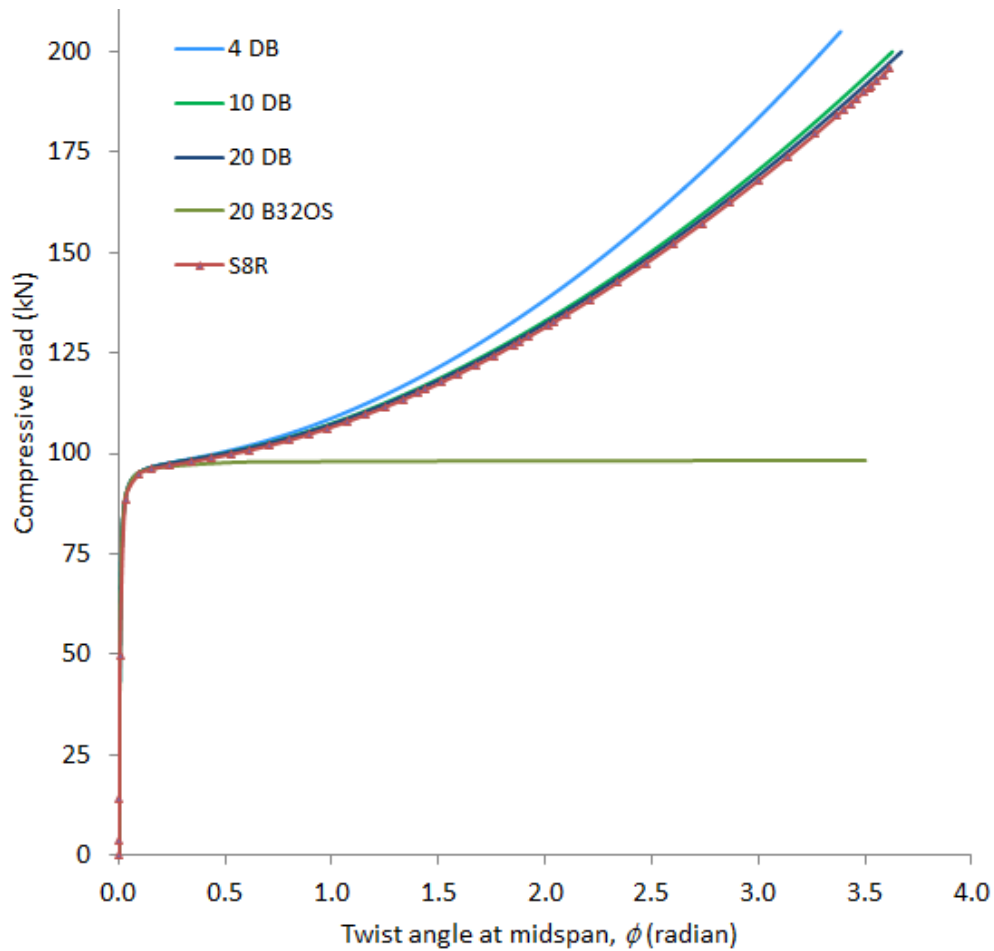
Figure 9 Torsional buckling behaviour of I-section column subjected to compressive load

As observed from Figure 9, the post-buckling behaviour predicted by the 20 DB elements agrees very well with the S8R shell model. Although the values corresponding to S8R shell element are slightly lower compared to the DB elements in the post-buckling range, the difference is negligible (difference being only 0.7% at 3.0 radians). Further, there is no significant difference between the behaviour predicted by the 10 DB elements and 20 DB elements implying that the solution has converged. The B32OS beam element in Abaqus, however, does not depict any nonlinearity in the post-buckling range.

To provide a sense of large deformation experienced by the column in the post-buckling range, the final deformed state of the shell model (with mesh supressed) is shown in Figure 10. Here, the column is shown with midspan twisted by 206° from its initial configuration.
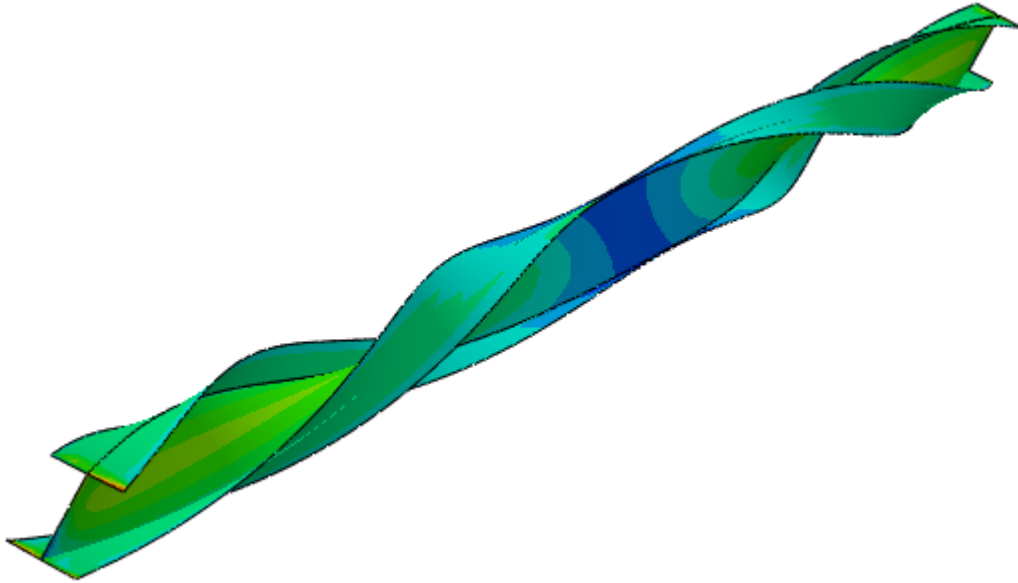
Figure 10 Final deformed state of I-section column (ϕ=206°)

The critical buckling load for the torsional buckling of column subjected to axial compression is given by [15, 16]:

$$N_x = (GJ + \pi^2 EI_w / L^2) / \mathrm{r}_2^2 \tag{69}$$

where $\mathrm{r}_2^2 = (I_y + I_z) / A + y_0^2 + z_0^2$. Using the properties from Table 1, the elastic torsional buckling load is calculated as 98.0 kN. As observed from Figure 9, the post-buckling path begin to start somewhat near this value but the exact buckling load is difficult to pinpoint due to continuous increase of load in the post buckling range.

The same column is also analysed for the flexural bucking mode when subjected to axial compressive force at its ends. Here the initial imperfection was created by performing linear static analysis for a small lateral load (~10 N) acting at the midspan, normal to the longitudinal axis of column in the weak axis direction. The nonlinear analysis was performed after the axial compressive loads were applied at the two ends.

The load-deformation responses describing the post-buckling behaviour of the column modelled with different elements are shown in Figure 11. It is observed that 4 numbers of DB elements are inadequate to define the post-buckling behaviour for such long column although they appear to be enough to predict the elastic buckling load. In fact, it would require 20 or more DB elements to adequately define the post-buckling behaviour of the column. In general, it was found that it usually required element size less than or equal to 200 mm for the convergence of solution. In this particular case, the buckling behaviour of B32OS elements and EB elements appear to be identical as indicated by the plots which superimposed on each other. The 30 DB elements also predicted the load-deformation response similar to B32OS element.

All numerical models predicted the elastic buckling load of 11.6 kN, measured at the lateral displacement of 280 mm. The theoretical critical buckling load for flexural buckling about y-axis is 11.57 kN, calculated using the expression $N_y = \pi^2 EI_y / L^2$ and the section properties from Table 1.
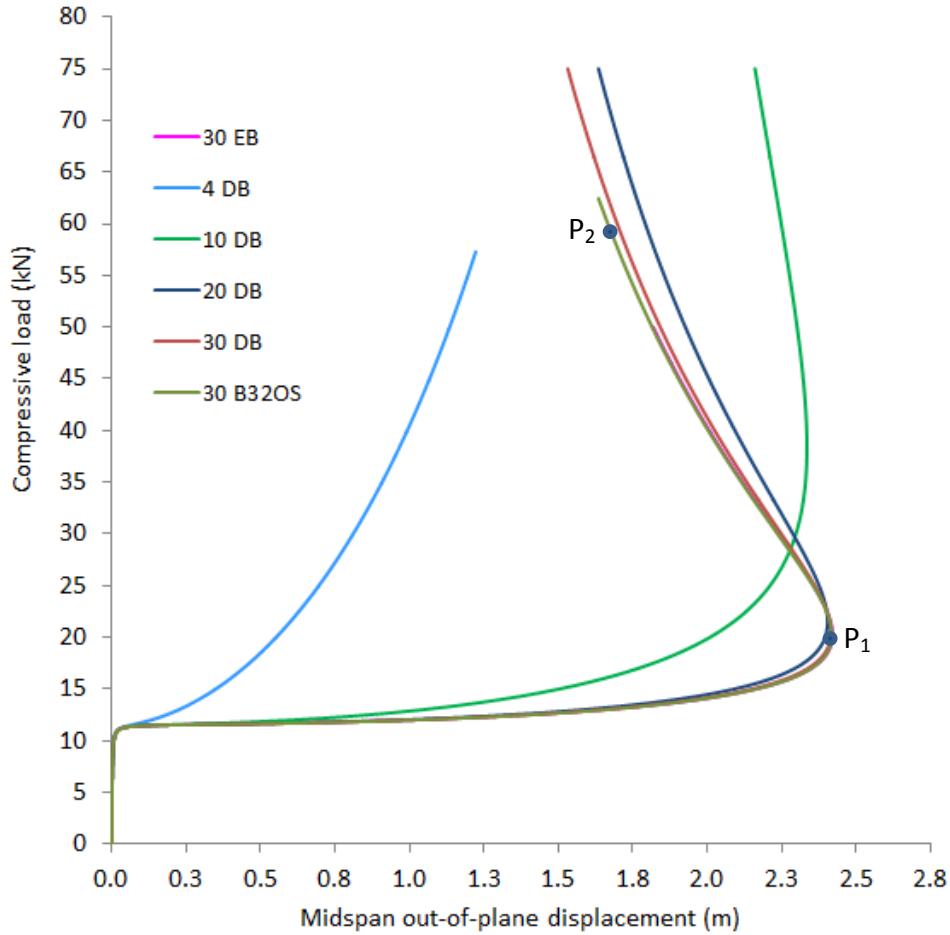
Figure 11 Flexural buckling behaviour of I-section column subjected to compression

The extent of deformation in the post-buckling range for the column undergoing flexural buckling about minor axis is depicted in Figure 12. It was observed that the column reached the maximum lateral displacement of 2.42m at a load of 20.4 kN (Figure 12a). Thereafter, the lateral displacement began to decrease and a stage is reached when two ends crossed each other and parts of the column started to experience tension as shown in Figure 12b. These deformation states are indicated by points P_1 and P_2 on Figure 11.

(a) Maximum lateral deformation(P_1)   (b) Final state of deformation(P_2)
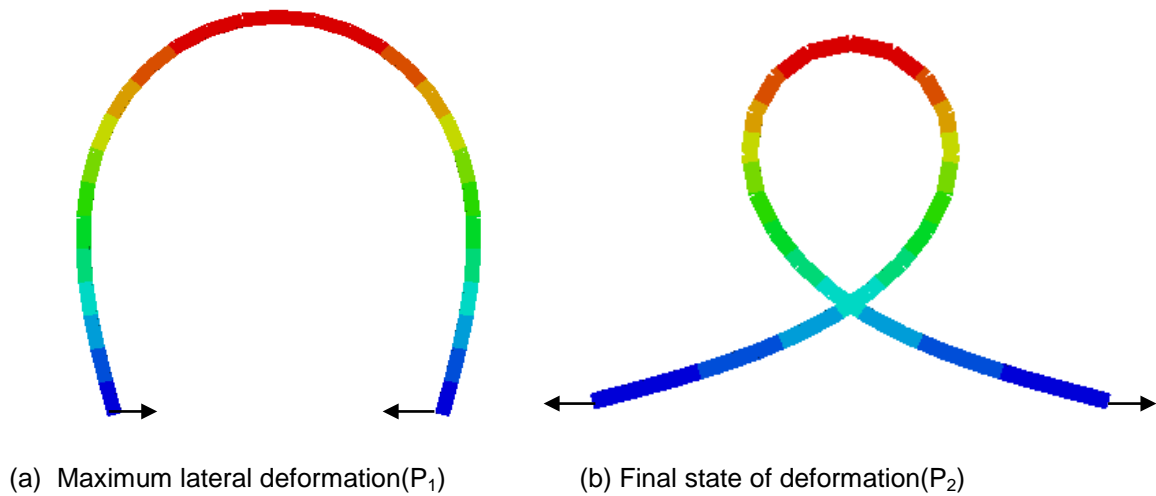
Figure 12 Deformation of B32OS column model in the post-buckling range

4.1.2   I-section beam subjected to major axis bending

A 4m long simply supported I-beam subjected to major axis bending and its buckling behaviour is presented in this example. The analytical model of the beam is shown in Figure 13. The boundary conditions applied to the beam are same as described in the proceeding Section. By adopting such boundary conditions for beam in bending, it allowed lateral buckling to occur symmetrically about the midspan. This minimizes the unbalanced constraint at the supports for the shell model which are quite sensitive to the boundary conditions at large deformation.

(a) Physical Model   (b) Analytical Model
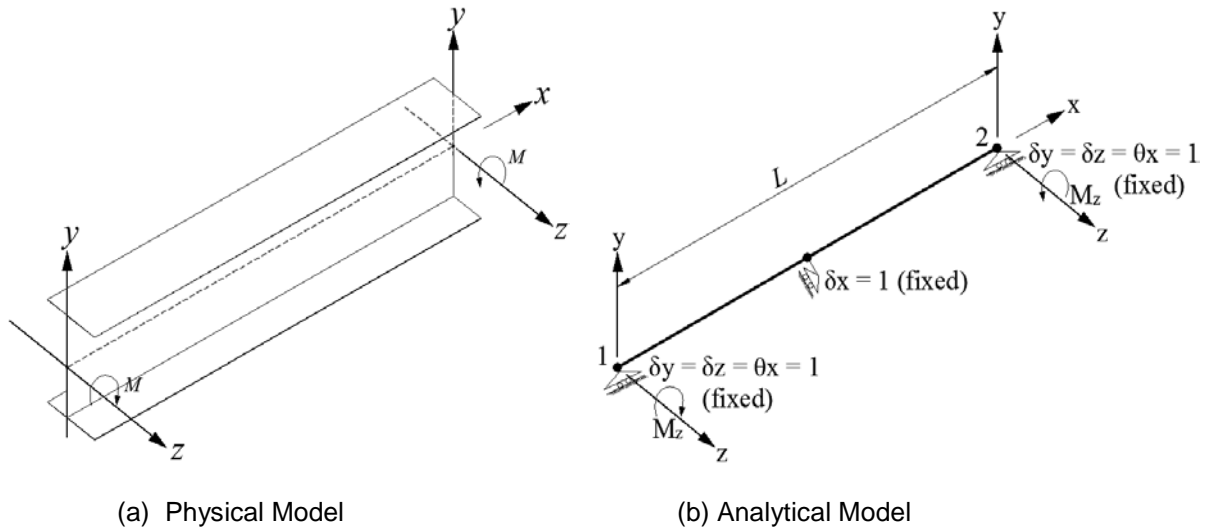
Figure 13 I-beam subjected to major-axis bending

Initial perturbation is induced to the beam by performing linear static analysis with the torque of 970 Nmm acting at the midspan of the beam about the longitudinal axis. Subsequently, nonlinear analysis is performed with equal end moments applied at the two ends. The incremental iterative force procedure is used for obtaining the load factors and corresponding displacements in OpenSees. The model is analysed using 4, 10, 20 DB elements and 30 EB elements in OpenSees, and 20 B32OS and 2400 S8R shell elements in Abaqus.

For the S8R shell model, the initial perturbation in the form of torque about longitudinal axis was achieved by applying lateral force at the top and bottom flange-web junctions normal to the beam axis. They were allowed to follow the nodal rotations. The end moments were first converted into stresses and then applied as the shell edge loads on to the cross-section at the ends. The boundary conditions were applied to the reference nodes defining the rigid body constraint which consisted of three small areas (usually 2mm by 4mm) located at the centre of web, at the top and bottom flange-web junctions. As the top and bottom flanges were developing high stress concentration and thus stiffening the model, the DoFs in the y-direction was released for the rigid body constraints located on the flange-web junctions.

The post-buckling behaviour predicted by the respective finite element models are presented in Figure 14 and Figure 15.
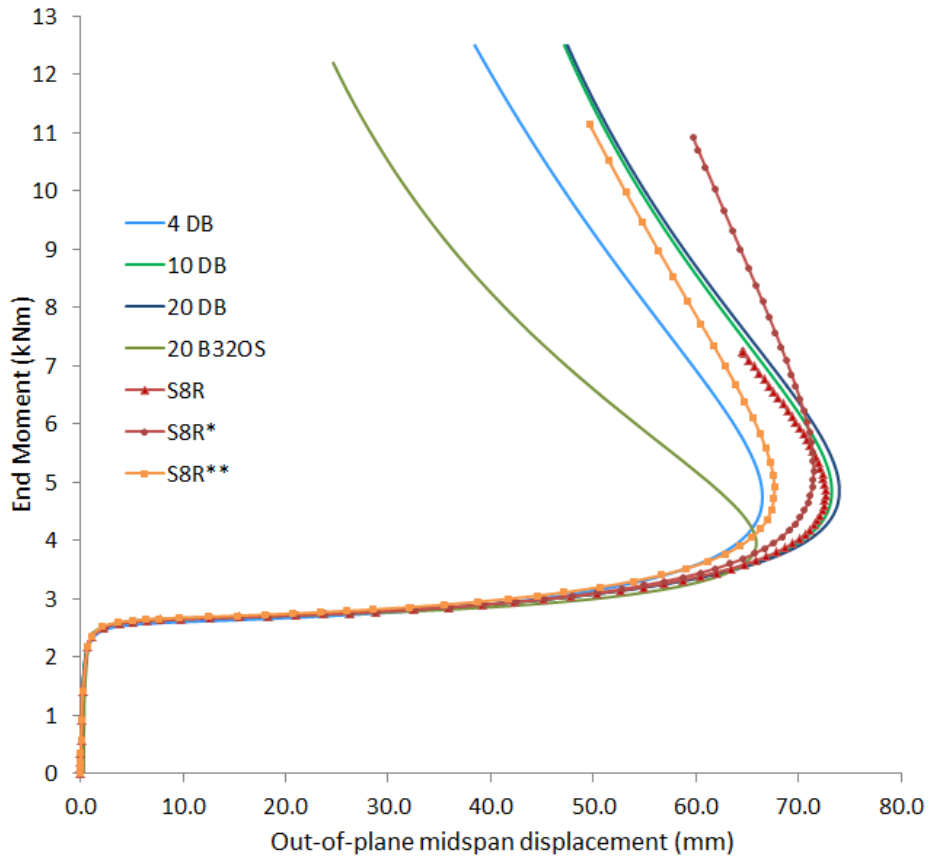
Figure 14 End moment vs out-of-plane midspan displacement for I-beam in major axis bending
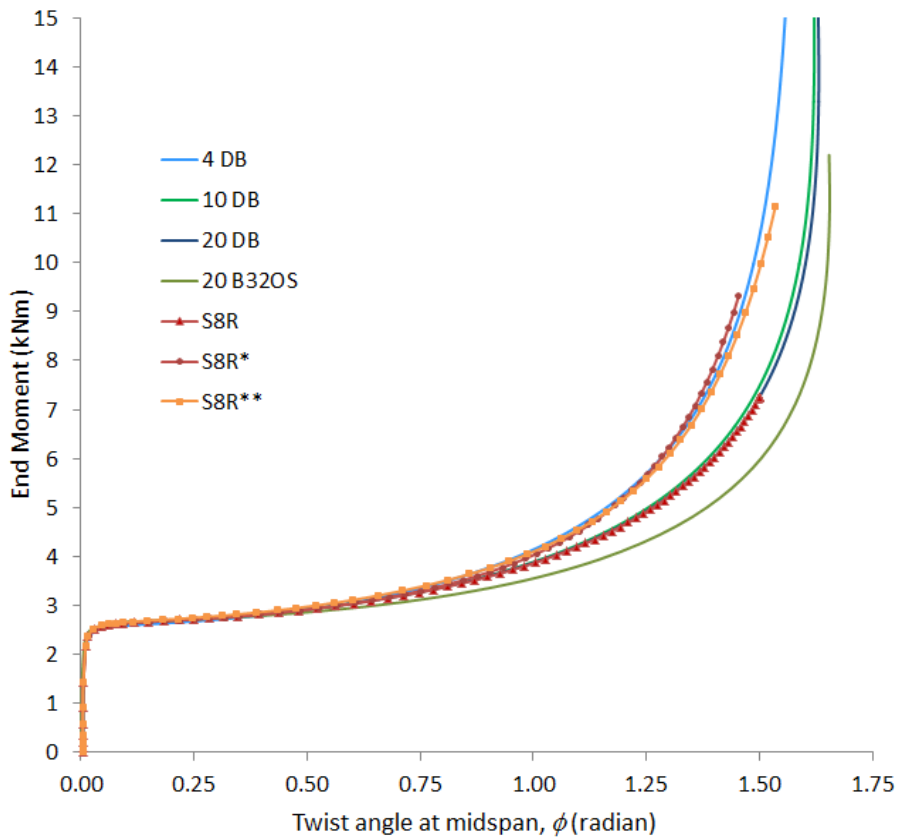

Figure 15 End moment versus twist angle at midspan for I-beam in major axis bending

The plot corresponding to S8R* is the case where same boundary condition has been applied to all three rigid body constraints located on web and flanges. The plot of S8R** corresponds to the case where the boundary condition is applied to the entire cross-section at the supports. As evident from the graphs, it has the effect of stiffening the model. This demonstrates that getting the right boundary conditions at the support is crucial for the correct prediction of post-buckling path in shell model at large displacement.

The critical buckling moment for an I-beam subjected to the major axis bending, which includes the effect of pre-buckling deformation is given by [22]:

$$M_{cr} = \frac{\pi}{L} \frac{\sqrt{EI_y GJ\left(1 + \frac{\pi^2 EI_\omega}{GJL^2}\right)}}{\sqrt{\left(1 - \frac{EI_y}{EI_z}\right)\left[1 - \frac{GJ}{EI_z}\left(1 + \frac{\pi^2 EI_\omega}{GJL^2}\right)\right]}} \tag{70}$$

Based on equation (70) and the section properties from Table 1, the classical buckling moment is calculated and presented along with the numerical solutions in the Table 2 below.

Table 2 Comparison of buckling moment for I-beam

Solution Type	Elastic buckling moment (kNm)
Classical (Eq.70)	2.690
10 DB	2.682
20 DB	2.691
20 B32OS	2.689
S8R shell	2.685
S8R shell*	2.449

*from elastic buckling analysis

In the above Table, the buckling moments from the numerical analyses were determined corresponding to the 15mm out-of-plane displacement at the midspan. This is the point at which the classical buckling moment (determined from equation(70)) intersects with the graphs. The buckling moment from the Abaqus elastic buckling analysis is lower by 9 percent than the ones predicted by the numerical analyses as it does not include the pre-buckling deformation. The buckling moments for a beam with pre-buckling deformation are found to be generally higher than those obtained from the Eigenvalue solution.

4.2   Monosymmetric Sections

4.2.1   Channel column subjected to compressive load

Buckling and post-buckling behaviour of a 6m long simply supported channel column subjected to compressive loads at the two ends is presented. The column with the boundary conditions is shown in Figure 16. The cross-section of the column is shown in Figure 7b.

A two-step analysis is followed to study the post-buckling behaviour. In the initial step, torsional imperfection is introduced in the model by performing linear static analysis with small magnitude of torque (485Nmm) acting at the midspan about the longitudinal axis. In the second step, reference compressive load with magnitude slightly above the buckling load is applied at the two ends and nonlinear analysis is performed with incremental iterative displacement controlled procedure. Here, the displacement controlled method has to be employed as the load has to pass through the

maximum point in the post-buckling range. Use of force-controlled method would result in numerical instability in this case.

(a) Physical Model   (b) Analytical Model
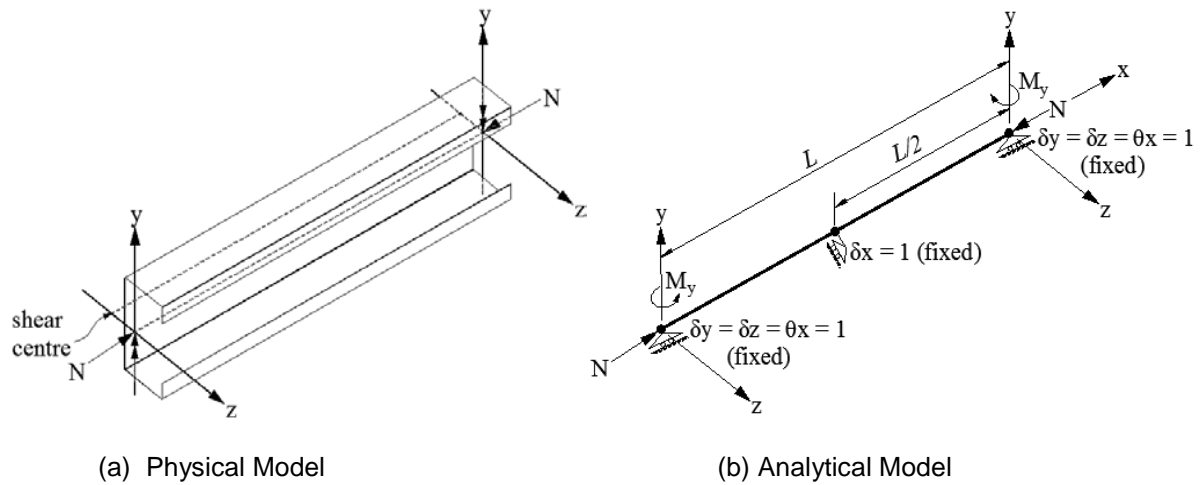
Figure 16 Channel column subjected to compression

Since the shear centre is eccentric to the centroid, the shifting of axial load to the centroid from the shear centre generated a couple equivalents to the axial load times the shear centre distance from the centroid. Hence, the couple is applied at each end about the minor axis to account for this eccentricity. These couples act simultaneously with the compressive force at the ends.

For the Abaqus S8R shell model, the initial perturbation in the form of torsional deformation is achieved by applying equal but opposite lateral force of 5N tangent to the centre of flanges and carrying out linear static analysis. This small force is allowed to follow the nodal rotation during the subsequent deformation so that it always maintains its direction tangent to the flanges. Next the reference compressive load is applied to the cross-section of the shell model as shell edge load. Nonlinear analysis is performed using Riks method.

The boundary conditions were modelled by creating three small areas: one at the centre of web and other two on each flange. These areas are assigned with the rigid body constraints. The boundary conditions were applied to these rigid body elements instead of applying to the whole cross-sections. Such type of manipulations was necessary to avoid constraining the model at the supports. By adopting such model of boundary condition, excellent agreement of the results were obtained. The only disadvantage with this method is that the small areas, on which rigid body element are assigned, are required to be created by partitioning the model. As such it introduces unnecessary small elements at the supports and along the member length coinciding the location of these areas. This, however, is found to have negligible influence on the final numerical solutions.

The discretization of the shell model itself consisted of 300 elements along the length, 4 elements for corners, 4 elements for web, 3 elements for flanges and 1 element for lips resulting in 8400 elements. This does not include the small elements which got created unavoidably due to the partitioning of whole model, which are required for creating the rigid body area to assign the boundary conditions as described above.

The post-buckling behaviour predicted by different elements is shown in Figure 17 where compressive force is plotted against the twist rotation at the midspan. In fact, in most of the examples to follow, twist rotation at the midspan has been used as variable for plotting the post-buckling path as it is found to be most convenient compared to other DoFs.

As observed from Figure 17, the post-buckling paths depict the softening behaviour with increasing displacement. The post-buckling path of B32OS significantly deviates from others beyond the buckling load. The post-buckling path of DB elements is smooth and decrement is gradual, as is the case of S8R shell model implying the perfect agreement between the two.
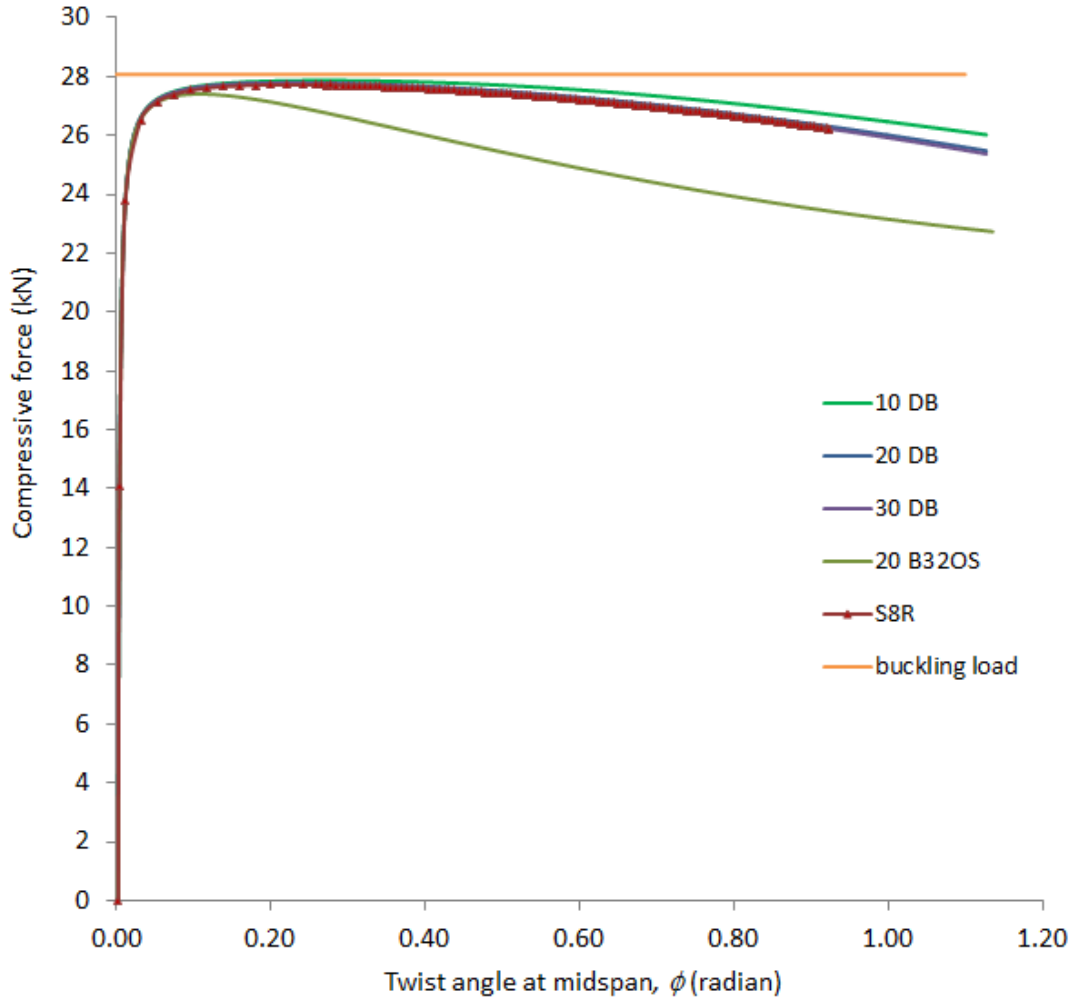
Figure 17 Post-buckling behaviour of channel column subjected to compression

The critical buckling load for a simply supported mono-symmetric section subjected to compressive load and undergoing flexural-torsional buckling is given by [16]:

$$N_{cr} = \frac{(N_x + N_z) - \sqrt{\left\{(N_x + N_z)^2 - 4N_x N_z r_0^2 / \left(r_0^2 + z_0^2\right)\right\}}}{2r_0^2 / \left(r_0^2 + z_0^2\right)} \tag{71}$$

in which,

$$N_z = \pi^2 EI_z / L^2$$
$$r_0^2 = (I_y + I_z) / A \tag{72}$$

The critical buckling load for this column is calculated as 28.07 kN. As observed from the graph, all numerical solutions reached the peak load (27.77 kN for 30 DB element, 27.41 kN for B32OS

element, and 27.73 kN for S8R shell element) and began to decrease as the deformation proceeded further. It is interesting to note that they never reach the critical buckling load.

4.2.2   Channel beam subjected to major axis bending

In this example, a 4m long channel beam is subjected to major axis pure bending with equal moments applied at the two ends (Figure 18a). The analytical model is shown in Figure 18b. The ends of the beam are free to warp and free to rotate about y and z axes while rotation is restrained about the x-axis. The translation in x-direction is restrained at midspan of the beam. This was arrived at after having noticed unequal development of stress distribution at the supports in the Abaqus shell model which was used to verify the post-buckling behaviour of DB elements. By restraining the longitudinal translation at the midspan, it resulted in symmetric deformation about the midspan and developed identical stress distribution at the two supports.

An imperfection is introduced by applying a torque of varying magnitude (depending on the type of deformation examined as explained below) at the midspan of the beam about the longitudinal axis. Next the reference end moments are applied at the two ends and nonlinear analysis is performed to determine the post-buckling behaviour.

For the S8R shell model, the boundary conditions were similar to the one described in Section 4.2.1. However, the discretization of the model consisted of 200 elements along the length, 4 elements each at the corners and web, 3 elements in each flange and 1 element in each lip resulting in 5600 elements for the whole model. Again this does not include the small elements created as a result of partitioning of model to form small areas required for the application of rigid body constraints for the boundary conditions.

(a) Physical Model   (b) Analytical Model
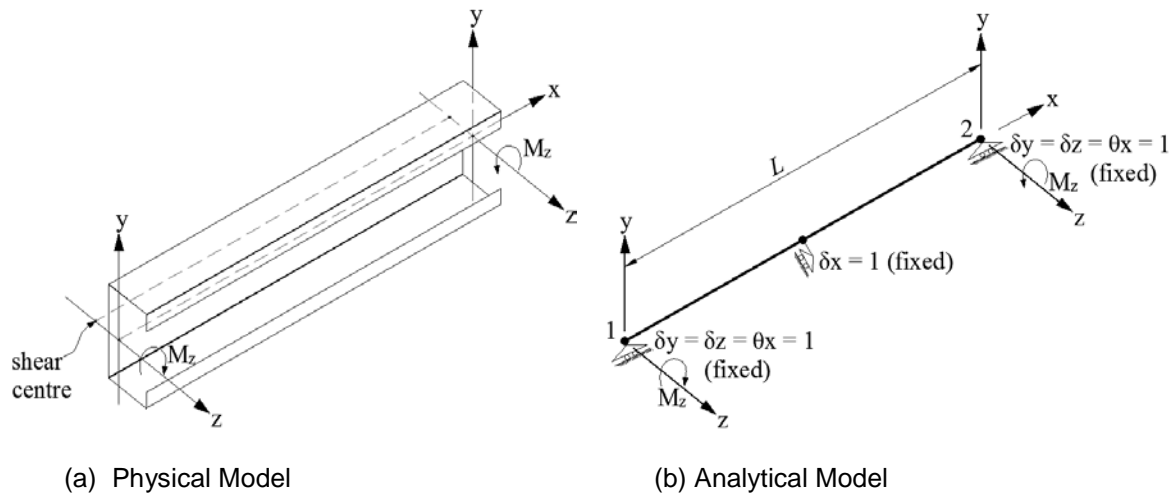
Figure 18 Channel beam subjected to major axis bending

For a channel beam under pure bending about major axis, it has been observed that the buckling path is dependent on the direction of initial perturbation torque (or initial twist rotation) applied to the beam. Figure 19 shows the plot of end moment versus twist angle at the midspan using varying magnitude and direction of twist applied during perturbation stage. The right-side branch of the plot is obtained with initial positive torque of 2,425 Nmm while the left-side branch for 20 DB and S8R corresponds to negative torque of 11,640 Nmm. This magnitude of torque has been determined such that it is just sufficient to make Abaqus shell model undergo small torsional deformation during the first stage of analysis. To observe the influence of initial imperfection magnitude, negative torque of 400 Nmm is also considered for the plot corresponding to 10 DB element. The plot obtained from Abaqus B32OS

beam model is also presented. In this case, the y, z axes of the beam has been shifted to the shear centre.

Any nonlinear analysis method can be employed to obtain the right-hand side plot as the moments are continuously increasing with the increasing deformation. However, for the left-hand side plot, it is necessary to engage Riks method as it would allow the maximum point to pass without undergoing numerical instability and related convergence issue.

For positive initial twist rotation, the equilibrium path is stable as indicated by the rising curve. Here, the load required to maintain equilibrium after buckling increases with increasing deformation.
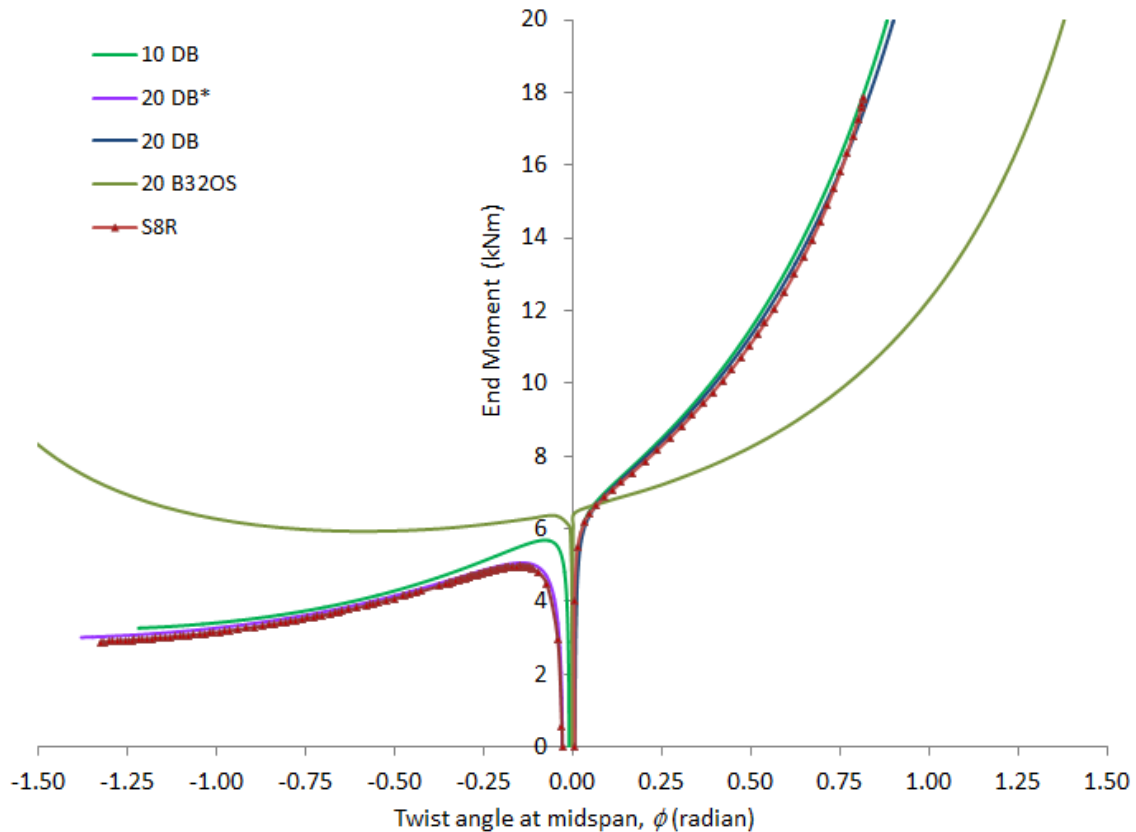

Figure 19 Asymmetric bifurcation of channel beam under major axis bending

For a negative initial torque at the midspan of beam, equilibrium path is unstable as indicated by the falling curve. In this case, the load required to maintain equilibrium after buckling decreases with increasing deformation. Further, when force-controlled method is used, the system became unstable after reaching the peak load and snapped to a very deformed state. The use of arc-length integrator enabled the detection of portions of the imperfect path which the force controlled method was not able to do so. This asymmetric behaviour of channel section was also observed using EB model. However the rate of numerical convergence was slow and worked only with very small (~1 Nmm) initial perturbation torque.

Based on the above, the post-buckling behaviour of channel beam in major axis bending depends on the sign of initial deformation. Hence, we may surmise that the channel section exhibits asymmetric bifurcation under major axis bending.

4.2.3   Channel beam subjected to minor axis bending

The same channel beam used in the above example is bent about the minor axis with equal end moments applied at the two ends. The end moments are applied such that the shear centre side is in tension while the lip is in compression. The boundary conditions along with applied end moments are shown in Figure 20. The boundary conditions are similar to the preceding example.

a)   Physical Model

(b) Analytical Model
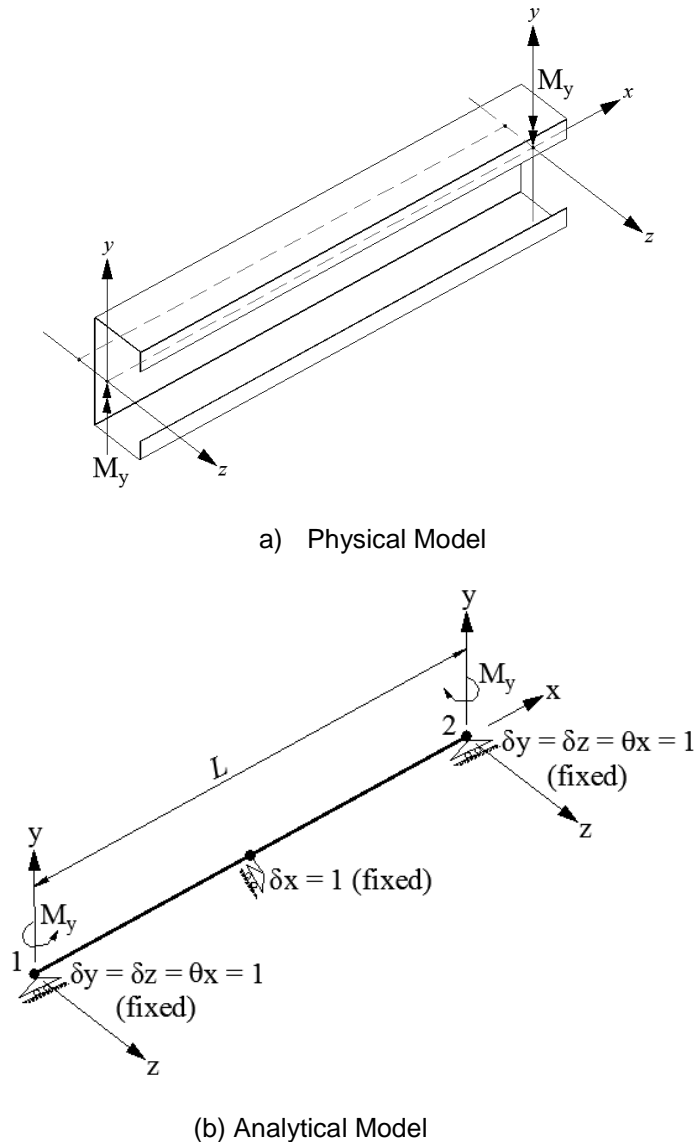
Figure 20 Channel beam subjected to minor axis bending

Following the two-step analysis process, the force-deformation responses are obtained from the nonlinear analysis with displacement-controlled procedure and are plotted in Figure 21. The initial perturbation was achieved with the application of torque equal to 485 Nmm applied at the midspan followed by the static analysis. For the S8R shell model, the similar method employed in the preceding examples has been followed for modelling the load and the boundary conditions.

As observed from Figure 21, the post-buckling path predicted by DB element agrees very well up to the twist angle of 1.0 radian. The slight discrepancy beyond this point is due the difficulty of reproducing the exact boundary condition for the shell model as it is observed to be sensitive at large displacement.

To determine the change in response influenced by the boundary conditions at the support, the same shell model was analysed with boundary conditions applied on the whole cross-section at the supports. The plot of S8R* corresponds to this case in Figure 21. As can be observed, there is marked difference between the post-buckling paths predicted by the same model with different simulations of boundary conditions at the supports.
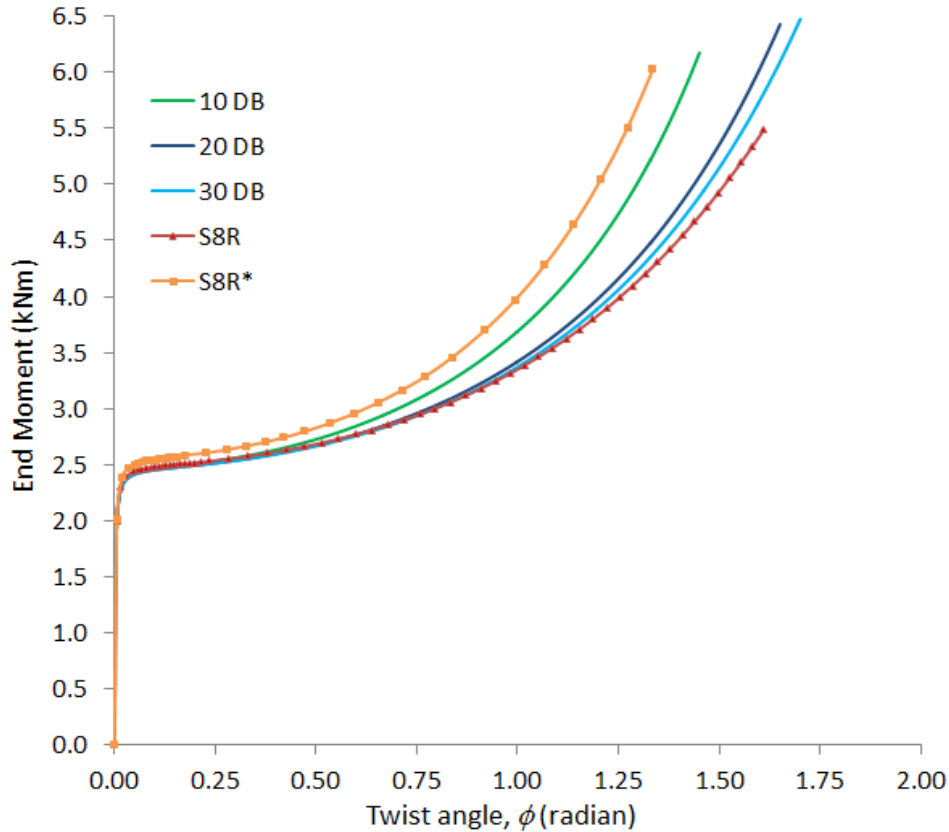

Figure 21 Post-buckling behaviour of channel beam subjected to minor axis bending

4.2.4   Cantilever channel beam subjected to torque at free end

In this example, a 3m long cantilever channel beam having cross-sectional dimension similar to Figure 7b but with thickness of 1.5 mm is subjected to end torque (Figure 22). Except for the warping DoF, all other DoFs are restrained at the support. The torque is applied at the free end.

For solving this problem, displacement-controlled iterative procedure is used whereby the twist angle at the free end has been controlled. The force-deformation relations are shown in Figure 23.

In this particular example, the only force in action within the beam is torque. Hence, the Wagner terms in equation(7) are not mobilized in the case of the elastic beam-column element. This has resulted in the linear relationship between the torque and the twist angle irrespective of their magnitude. However, the plot of displacement-based beam element exhibits the nonlinear curve which gradually stiffens with increasing torque. This is made possible mainly due the presence of Wagner term in the strain formulation in displacement-based element. The similar stiffening behaviour has been observed by Zhang [9] in doubly-symmetric section and by Battini and Pacoste [7] in narrow rectangular sections.
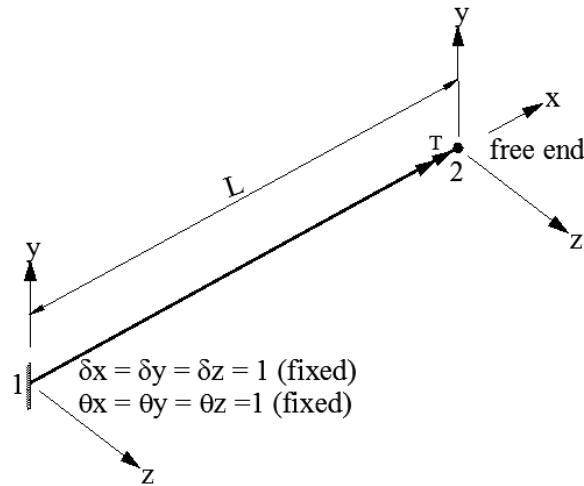
Figure 22 Cantilever channel beam subjected to torsion at the free end
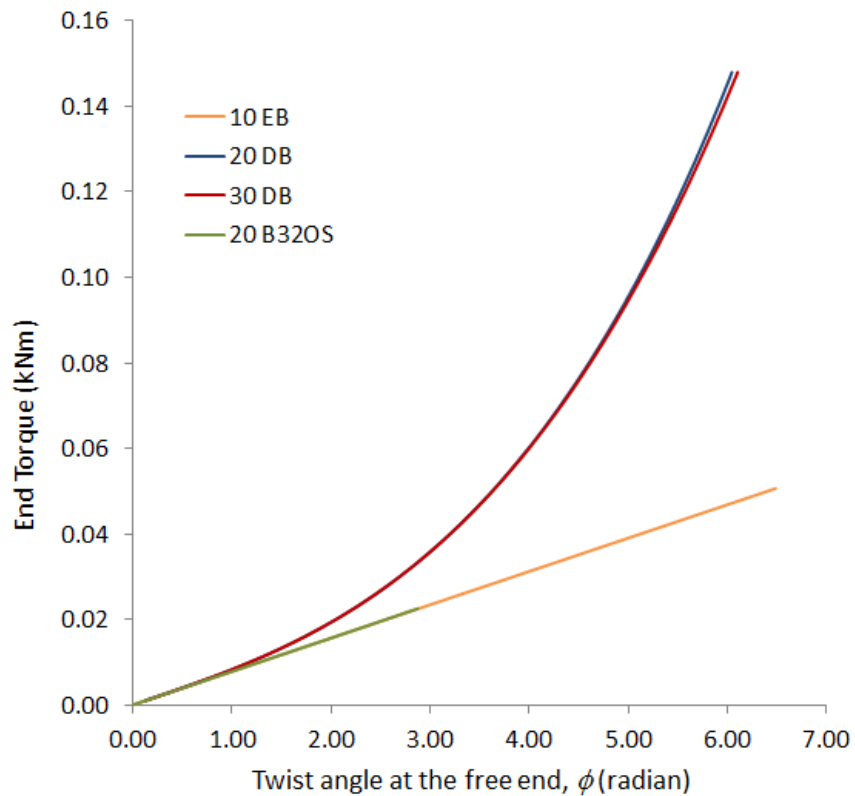
Figure 23 Torsional response of channel beam

Interestingly, the B32OS does not depict any nonlinearity in this case. From the above plot, it shows that the displacement-based beam elements may be used to predict the accurate results for large displacement analysis where the torsional effects are significant. It further proves that the co-rotational framework in itself does not produce any non-linearity where the predominant load is torsion. Furthermore, the fact that the section undergoes large torsional deformation even with small magnitude of torsion further validates the claim that thin-walled open sections possess very low torsional resistance.

4.3 Asymmetric Section

4.3.1 Asymmetric section column subjected to compressive load

In order to demonstrate the capability of the DB elements in analyzing the thin-walled beam having general cross-sections, a variant of channel section, with upper lips turned upwards has been used as representative of the typical asymmetric sections. In this example, a 6m long column having asymmetric cross-section (Figure 7c) is subjected to compressive force at its two ends. The boundary conditions are same as the model in Figure 16. The physical model is shown in Figure 24.
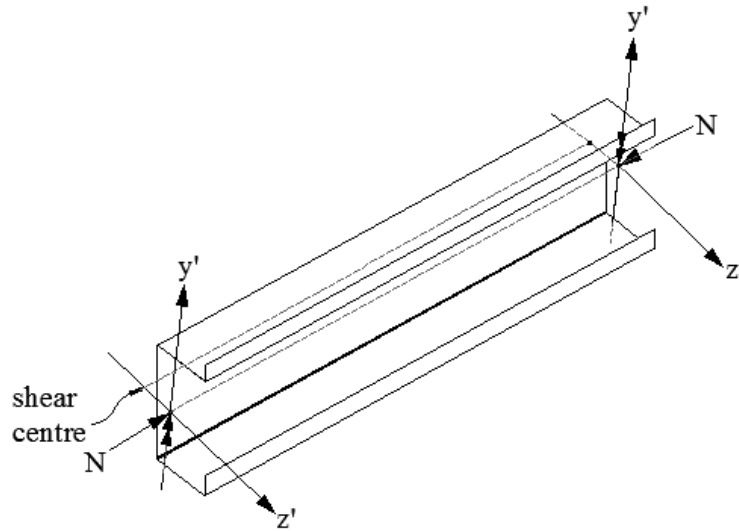

Figure 24 Asymmetric section column subjected to axial compression

Similar to the process followed in the preceding examples, the initial perturbation in the form of twist was applied at the midspan followed by the linear static analysis. For the S8R shell model, because of the unequal distance to the top and bottom flange from the centroid, the lateral force of 5.09 N on the centre of top flange and 4.91 N on bottom flange has been applied to cause the initial twist. Subsequently, the post-buckling load-deformation response was obtained through the nonlinear analysis for the reference compressive load applied at the two ends. The buckling paths are shown in Figure 25.

As observed from Figure 25, the load-deformation path is similar to the post-buckling behaviour of monosymmetric channel column. This is expected since the asymmetric section is a variant of the channel beam section. Further the plot of 20 DB and 30 DB elements superimposed on each other implying that the solution has converged.

For asymmetric sections such as the column in this example, the critical buckling load can be determined numerically as the lowest root of the polynomial equation [15, 16]:

$$f(N) = N^3\left(r_2^2 - y_0^2 - z_0^2\right) - N^2\left[\left(N_x + N_y + N_z\right)r_2^2 - N_y z_0^2 - N_z y_0^2\right]$$
$$+ Nr_2^2\left(N_x N_y + N_y N_z + N_z N_x\right) - \left(N_x N_y N_z r_2^2\right)$$

(73)

Using the properties given in Table 1, the elastic buckling load is calculated as 26.75 kN. This theoretical buckling load is found to be always less than the lowest of N_x, N_y, N_z and corresponds to a flexural-torsional mode [16]. Unlike the monosymmetric channel column, in this case all the numerical solution reached the peak load slightly above the buckling load after which they began to decrease as the deformation progressed.
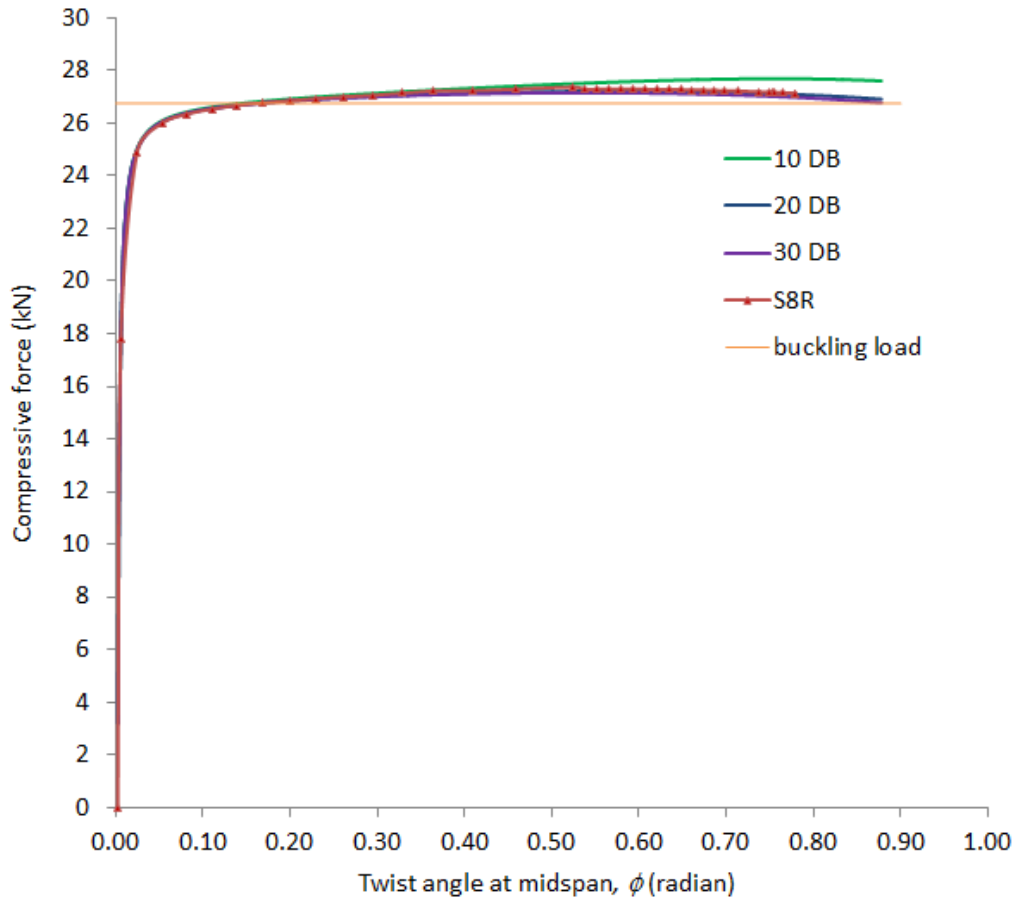
Figure 25 Load-deformation response of asymmetric section column

4.3.2   Asymmetric section beam subjected to pure bending

A 4m long beam with asymmetric cross-section is subjected to bending about its major principal axis. The process of obtaining the numerical solution and the boundary conditions adopted are similar to the monosymmetric channel section in major axis bending.

However, the S8R shell model was transformed through rotation such that the principal axis of the cross-section coincided with the rectangular axis. The load and boundary conditions were applied with respect to the principal axis system. Based on the performance of S8R shell model, the initial twist required to perturb the beam at the onset of nonlinear analysis was determined such that the rotational DoF (about the longitudinal axis at the midspan) was +0.007 radians. The post-buckling path is presented in Figure 26.

As observed from Figure 26, the post-buckling behaviour of asymmetric section beam subjected to the major principal axis bending depicted by DB element and S8R shell model agree well.

The same beam is also subjected to the minor axis bending following the similar procedure used for the minor axis bending of channel beam. The beam is bent such that the shear centre side is in tension. Here the initial twist required to perturb the beam was determined such that the rotational DoF at the midspan of the beam was -0.004 radians. The load-deformation response is plotted in Figure 27.

Here in this case, the initial portion of post-buckling path agree well but start to differ at the large displacement range (beyond -0.75 radians). The plausible cause of the difference is due to the difficulty of representing the exact boundary conditions in shell model.
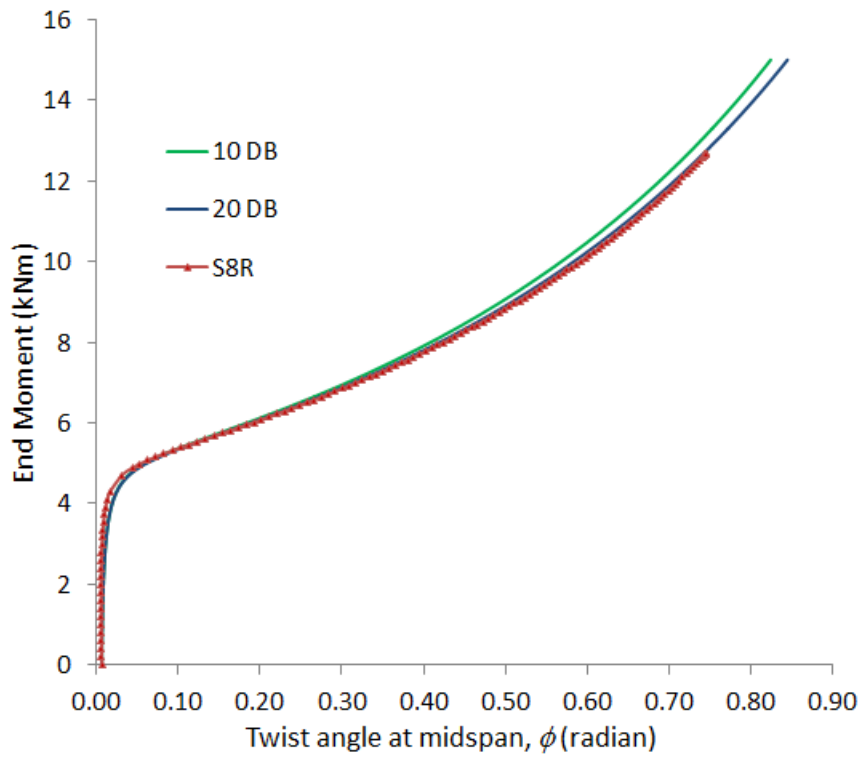
Figure 26 Post-buckling behaviour of asymmetric section beam subjected to major principal axis bending
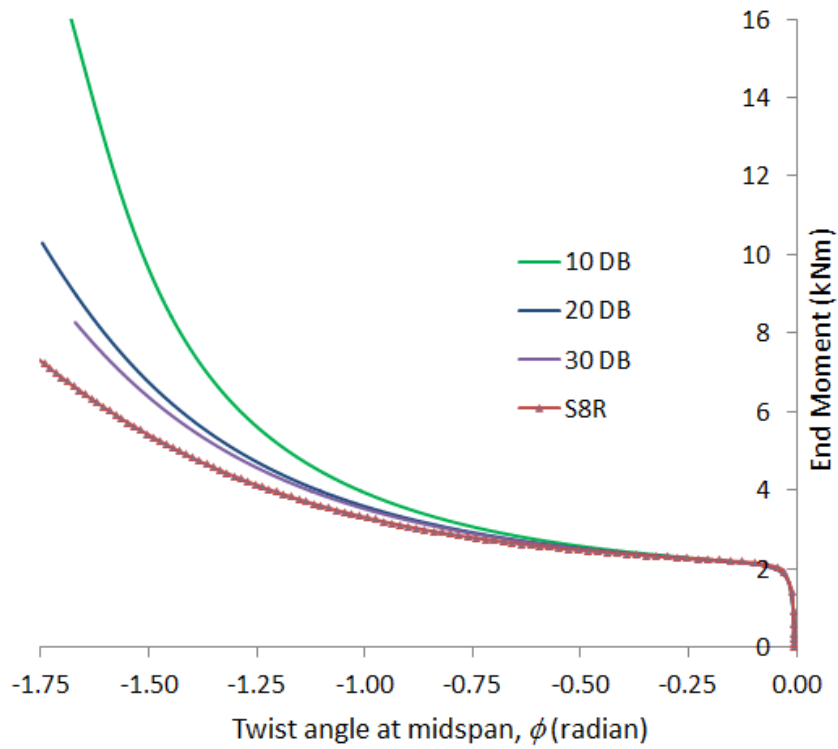
Figure 27 Post-buckling behaviour of asymmetric section beam subjected to minor principal axis bending

Based on the forgoing examples, it has been observed that the post-buckling behaviour of S8R shell element is dependent on the way the boundary conditions are imposed at the support. For instance, when whole cross-section at the support is restrained, the nonlinear behaviour tends to initiate earlier in the post-buckling range. Although the problem has been overcome to certain extent by employing the rigid body constraint for the boundary conditions, the representation of exact boundary conditions in shell element is nevertheless a challenging issue in itself. Hence, in the large displacement range, the solutions obtained from the DB element and those from the S8R shell elements show some differences. Additionally, the distortion of the cross-section at the large displacement in the shell model is bound to occur but the DB elements are formulated assuming that it retains its original shape throughout the deformation history. This might well be another factor contributing to the discrepancy between the behaviour of DB element and S8R shell element at large displacement.

In spite of the slight differences at the large displacement range, nonetheless the solutions were identical within the practical range of post-buckling. Further, in terms of efficiency in solving the numerical problem, the DB elements are found to be superior in speed compared to the S8R shell element. So, to demonstrate the fastness in solving the problem, execution time of DB and S8R shell elements is compared in Table 3. The comparison is based on the execution time required to solve the I-section column of Section 4.1.1.

Table 3 Comparison of execution time required for S8R shell and DB model

Items	S8R Shell element	DB Element
Number of analysis steps	150	2000
Execution time (seconds)*	2096	384
Execution time (seconds)/analysis step	13.97	0.192
CPU utilization	Above 45%	At 13%
Number of elements	3600	20

*Computer with processors Intel® Core™ i5-3337U CPU@1.8GHz

5. CONCLUSIONS

Formulation of general thin-walled (open section) beam-column finite element and its implementation in the OpenSees framework is presented. A simple cross-section transformation matrix relating the axial force acting at the centroid and the shear centre is developed within the local axis system which enabled the application of formulation to the general thin-walled sections.

The displacement-based beam-column element is capable of handling large deformation with beams having general cross-sections. Numerical examples demonstrated that DB elements are equally accurate with the Abaqus shell element. The slight discrepancies observed at the large displacement are due to the difficulty of replicating the exact boundary conditions in shell models. Although elastic beam-column element is developed based on linear theory and therefore requires more number of element for achieving equivalent accuracy, its capability to predict the true buckling load mainly arose due to the inclusion of Wagner effect in the torsional rigidity term.

As evident from the several examples highlighted in this report, the main advantage of using displacement-based beam-column lies in the fact that the problem can be solved much faster while providing very accurate solutions.

6. REFERENCES

1. Baigent, A.H. and G.J. Hancock, *Structural analysis of assemblages of thin-walled members.* Engineering Structures, 1982. 4(3): p. 207-216.
2. Hancock, G.J., *Portal frames composed of cold-formed channel and zed-sections, in Steel Framed Structures - Stability and Strength, (R. Narayanan, ed.).* 1985, Elsevier Applied Science Publishers, London, Chap. 8.
3. Rasmussen, K.J.R., *Bifurcation of locally buckled members.* Thin-Walled Structures, 1997. 28(2): p. 117-154.
4. Pi, Y.L. and N. Trahair, *Prebuckling deflections and lateral buckling. I: theory.* Journal of Structural Engineering, 1992. 118(11): p. 2949-2966.
5. Gruttmann, F., R. Sauer, and W. Wagner, *Theory and numerics of three-dimensional beams with elastoplastic material behaviour.* International Journal for Numerical Methods in Engineering, 2000. 48(12): p. 1675-1702.
6. Mo Hsiao, K. and W. Yi Lin, *A co-rotational formulation for thin-walled beams with monosymmetric open section.* Computer Methods in Applied Mechanics and Engineering, 2000. 190(8–10): p. 1163-1185.
7. Battini, J.-M. and C. Pacoste, *Co-rotational beam elements with warping effects in instability problems.* Computer Methods in Applied Mechanics and Engineering, 2002. 191(17–18): p. 1755-1789.
8. Alemdar, B.N., *Distributed plasticity analysis of steel building structural systems.* 2001, Georgia Institute of Technology.
9. Zhang, X., K.J.R. Rasmussen, and H. Zhang, *Formulation and implementation of three-dimensional doubly symmetric beam-column analyses with warping effect in OpenSees.*, in *Research Report R917.* 2011, School of Civil Engineering, Centre for Advanced Structural Engineering: University of Sydney.
10. Fenves, G.L., et al. *An object-oriented software environment for collaborative network simulation.* in *Proceedings of 13th World Conference on Earthquake Engineering. No. 1492.* 2004.
11. Vlasov, V.Z., *Thin-walled elastic beams.* 2 Edition ed. 1961, Jerusalem: Israel Program for Scientific Translations.
12. Crisfield, M.A., *A consistent co-rotational formulation for non-linear, three-dimensional, beam-elements.* Computer Methods in Applied Mechanics and Engineering, 1990. 81(2): p. 131-150.
13. Teh, L.H. and M.J. Clarke, *Co-rotational and Lagrangian formulations for elastic three-dimensional beam finite elements.* Journal of Constructional Steel Research, 1998. 48(2–3): p. 123-144.
14. McGuire, W., R.H. Gallagher, and R.D. Ziemian, *Matrix Structural Analysis.* 2 Edition ed. 2000: Faculty Books. Book 7.
15. Timoshenko, S.P. and J.M. Gere, *Theory of Elastic Stability.* 2 Edition ed. 1961: McGrawHill-Kogakusha Ltd, Tokyo.
16. Trahair, N.S., *Flexural-Torsional Buckling of Structures.* 1st Edition ed. 1993, London ; Melbourne: E & FN SPON. 360.
17. Zbirohowski-Koscia, K., *Thin Walled Beams- From theory to practice.* 1967, London: Crosby Lockwood & Son Ltd.
18. Papangelis, J.P. and G.J. Hancock, *Computer analysis of thin-walled structural members.* Computers & Structures, 1995. 56(1): p. 157-176.
19. Pilkey, W., *Analysis and Design of Elastic Beams–Computational Methods.* 2002: John Wiley & Sons, New York.

20. Lue, D.M., J.L. Liu, and C.H. Lin, *Numerical evaluation on warping constants of general cold-formed steel open sections.* International Journal of Steel Structures, 2007. 7(4): p. 297-309.

21. Simulia, D.S., *Abaqus Analysis User's Guide - Version 6.13*. 2013: Providence, RI, USA.

22. Vacharajittiphan, P., S.T. Woolcock, and N.S. Trahair, *Effect of In-Plane Deformation on Lateral Buckling.* Journal of Structural Mechanics, 1974. 3(1): p. 29-60.